Tectonics

RESEARCH ARTICLE
10.1029/2020TC006148

The Chimei Submarine Canyon and Fan: A Record of Taiwan Arc-Continent Collision on the Rapidly Deforming Overriding Plate

Yu-Huan Hsieh[1,2], Char-Shine Liu[2], John Suppe[1,3], Timothy B. Byrne[4], and Serge Lallemand[5]

[1]Department of Earth and Atmospheric Sciences, University of Houston, Houston, TX, USA, [2]Ocean Center, National Taiwan University, Taipei, Taiwan, [3]Department of Geosciences, National Taiwan University, Taipei, Taiwan, [4]Department of Geosciences, University of Connecticut, Storrs, CT, USA, [5]Geosciences Montpellier Laboratory, CNRS, Montpellier 2 University, Montpellier, France

Key Points:
- Rapidly deforming wedge-top Chimei Canyon/Fan on Philippine Sea plate shows distinctive wide-canyon morphology and rapid fan evolution
- Chimei Fan gives 0- to 2-Ma record of Taiwan arc-continent collision based on seismic stratigraphy and integration with proximal onshore record
- The Taiwan-derived depocenter shifted ~1 Ma from proximal forearc basin to east of arc due to ~60-km thrust-belt convergence and over filling

Supporting Information:
- Supporting Information S1

Correspondence to:
Y.-H. Hsieh, C.-S. Liu and J. Suppe,
luckyuki9@gmail.com;
csliu@ntu.edu.tw;
jsuppe@central.uh.edu

Citation:
Hsieh, Y.-H., Liu, C.-S., Suppe, J., Byrne, T. B., & Lallemand, S. (2020). The Chimei submarine canyon and fan: A record of Taiwan arc-continent collision on the rapidly deforming overriding plate. *Tectonics*, *39*, e2020TC006148. https://doi.org/10.1029/2020TC006148

Received 21 FEB 2020
Accepted 5 OCT 2020
Accepted article online 13 OCT 2020

Abstract The Chimei Canyon is a large, uplifting wedge-top submarine canyon offshore eastern Taiwan that has delivered sediment since ~1–2 Ma from the rapidly eroding Taiwan orogen to the Chimei Fan in the Huatung Basin, east of the colliding Luzon Arc. In this study, we document the depositional record of the Taiwan arc-continent collision on the adjacent oceanic Philippine Sea Plate using multichannel seismic reflection data together with high-resolution bathymetry data to study the morphology, seismic sequences, and structures of the Chimei Canyon-Fan system. The sedimentary strata are separated into three seismic sequences. The lowest sequence overlies oceanic crust, showing Cenozoic-Cretaceous pelagic seismic facies that we interpret as pre-collisional, whereas the middle and upper sequences are syn-collisional. We propose a model for the development of the Chimei Canyon-Fan in which the middle sequence first developed ~1–2 Ma, while the main depocenter was to the west in the forearc basin, west of the Luzon Arc. The upper sequence records a shift of depocenter after ~1 Ma from the forearc basin to the Chimei Fan east of the Luzon Arc. At the same time, this antecedent paleochannel-fan system was deformed rapidly (~60 mm/yr; 62 km minimum shortening) by a complex imbricate thrust belt with the emergence of the arc and forearc basin as the west-vergent Coastal Range thrust belt and the Chimei Canyon incising the active east-vergent Offshore East Taiwan thrust belt. The thrust belt underlying the wedge-top Chimei Canyon-Fan has undergone >19-km shortening and ~2.6-km structure uplift.

1. Introduction

Submarine fan systems provide good opportunities for obtaining integrated long-term records of on-land denudation history (Curray, 2014; Curray et al., 2003; Ingersoll et al., 2003; Normark & Carlson, 2003). Within plate convergent settings, mountain belts with high uplift rates often have high erosion rates that result in large sediment fluxes being transported through river and submarine canyon systems and into adjacent deep-sea fans (Normark & Carlson, 2003; Rise et al., 2013). The deep-basin sediments more broadly consist of pre-, syn-, and post-orogenic deposits (Alam et al., 2003), with sequence boundaries that are usually clear and widespread. Therefore, seismic stratigraphic mapping of these sequences provides a straightforward path to constrain broad features of the orogenic history. Furthermore, integrating the subaerial mountain belt with adjacent submarine fans provides unified insight into the entire depositional system, from source to sink, as demonstrated by the Bengal Fan studies (Alam et al., 2003; Curray, 2014). The Bengal Fan is the largest deep-sea fan in the world (Curray et al., 2003), composed of sediments eroded from the Himalayas and Tibetan Plateau in the India-Asia collision through the Cenozoic and deposited on adjacent Indian Ocean crust (Curray, 2014; Curray et al., 2003). In the present paper, we apply similar strategies to the very active and rapidly eroding Taiwan arc-continent collision, as recorded in the Chimei Canyon-Fan system, which is deposited on oceanic crust of the adjacent Philippine Sea Plate.

Chimei Canyon is one of the large submarine canyons offshore Taiwan. Its cross-sectional size and shape are comparable to the largest submarine canyons of the world and nearly identical to the giant Swatch of No Ground Canyon of the Bengal System (Figure 1). In contrast with the giant and long-lived Cenozoic Bengal-Himalayan system (>15 km proximal thickness, ~4,000 km long, ~50 Ma), the Chimei Canyon-Fan system and more broadly the Taiwan mountain belt are very young (<2 Ma for the Chimei Canyon-

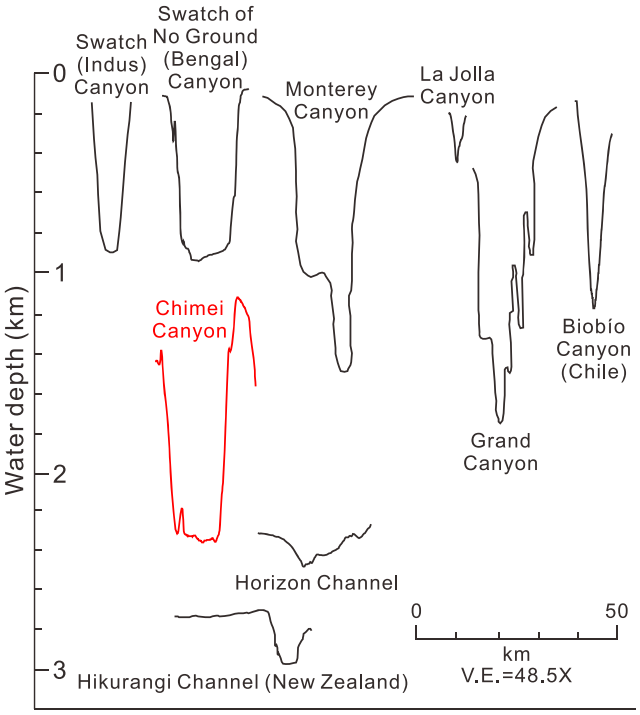

Figure 1. Comparison of Chimei Canyon in cross section with well-known submarine canyons in convergent-margin settings (except Grand Canyon). Vertical axis shows water depth. This figure is modified from Normark and Carlson (2003): Swatch Canyon (Shepard, 1973); Swatch of No Ground Canyon (Curray & Moore, 1974; Shepard, 1973); Monterey Canyon and Grand Canyon (Carlson & Karl, 1988); La Jolla Canyon (Shepard & Buffington, 1968); Biobio Canyon (Bernhardt et al., 2015); Horizon Channel (Stevenson & Embley, 1987); Hikurangi Channel (Mountjoy et al., 2018).

Fan system) and as small as the Swiss Alps (Taiwan ~380 km NS) but are characterized by very rapid rates of relevant geologic processes, thereby providing significant accessible research opportunities into active processes. The Taiwan mountain belt is currently one of the youngest and fastest arc-continent collisions in the world (Figure 2), with a present convergence of ~91 mm/yr between the Yangtze Block of the Eurasian Plate and the Philippine Sea Plate based on the GSRM v2.1 global plate model (Argus et al., 2011; DeMets et al., 2010; Kreemer et al., 2014). The Chimei Canyon-Fan (Figure 3a) straddles the most actively deforming part of the Taiwan collision zone, consuming two-thirds (~60 mm/yr) of the total plate convergence (Tsai et al., 2015; Wu et al., 2016). As such, the Chimei Canyon-Fan system can be considered an active wedge-top system, with tectonic uplift potentially playing a significant role in submarine canyon incision. Furthermore, critically, steep onshore topography reaching >3,000-m elevation and subtropical climate (on the average four typhoons per year and mean annual precipitation of 2.5 m/yr) together with frequent earthquakes (Dadson et al., 2003, 2004, 2005) have resulted in high erosion rates (4–5 km/my) since 2 Ma (Derrieux et al., 2014; Fellin et al., 2017), with large amounts of orogenic sediment delivered from the subaerial mountain belt through submarine canyons and into adjacent deep-sea submarine fans (Figure 2). The currently active onshore source region of the Chimei Canyon-Fan is shown in Figure 3a, with the antecedent Hsiukuluan River functioning as the transport pathway across the deforming Coastal Range thrust belt and into the offshore Chimei Canyon (Figures 3a and 4).

In offshore eastern central Taiwan, the bulk of the eroded sediment is fed through submarine canyons into the northwest corner of the Huatung Basin of the Philippine Sea Plate (Figures 2 and 3). The Huatung Basin is a nearly closed basin >4,000-m deep, with sediment transported out of the basin only in its northeastern corner where the Gagua Ridge enters the Ryukyu Trench (Figure 2). Therefore, most of the orogenic sediment coming from Taiwan into the Huatung Basin is trapped (Liu et al., 1997a; Schnürle et al., 1998), providing a record of the development of the Taiwan arc-continent collision. The submarine fan strata are deposited on top of a pre-collisional sequence, forming a widespread unconformity that we have used to constrain the volume of overlying orogenic sediment. Furthermore, because of plate convergence, proximal parts of the Chimei Fan have been incorporated into the easternmost thrust belt of the Taiwan collision, while the northeastern part of the Chimei Fan has been incorporated into the Ryukyu accretionary wedge (Figure 2). Studying the Chimei Fan thus can provide insight into the sedimentary processes and mass balance of this rapidly evolving source-to-sink system and also help to constrain the orogenic history of Taiwan mountain belt.

The structures and depositional history offshore eastern Taiwan have been relatively little studied, in contrast with the better-known onshore Taiwan mountain belt. In this study, high-resolution multibeam bathymetric data together with multichannel seismic reflection data have been used to (1) document the morphology of the Chimei Canyon-Fan system, (2) document and map the principal seismic facies and define three regional seismic sequences, (3) document the deformation and uplift associated with the formation of the Chimei Canyon, and (4) estimate the preserved volume and age of the Chimei Fan system and compare it with the estimated erosive flux of sediment from the on-land source area. Finally, we develop a model for the progressive eastward propagation of deposition and deformation of the evolving eastern Taiwan source-to-sink system during the Pleistocene.

2. Tectonic and Stratigraphic Settings

2.1. Tectonic Setting of Taiwan Arc-Continent Collision

The Taiwan arc-continent collision results from ongoing oblique convergence between the N-S Luzon Arc and NE–SW Eurasian Margin (Figure 2) (Angelier et al., 1986; Barrier & Angelier, 1986; Biq, 1972; Bowin

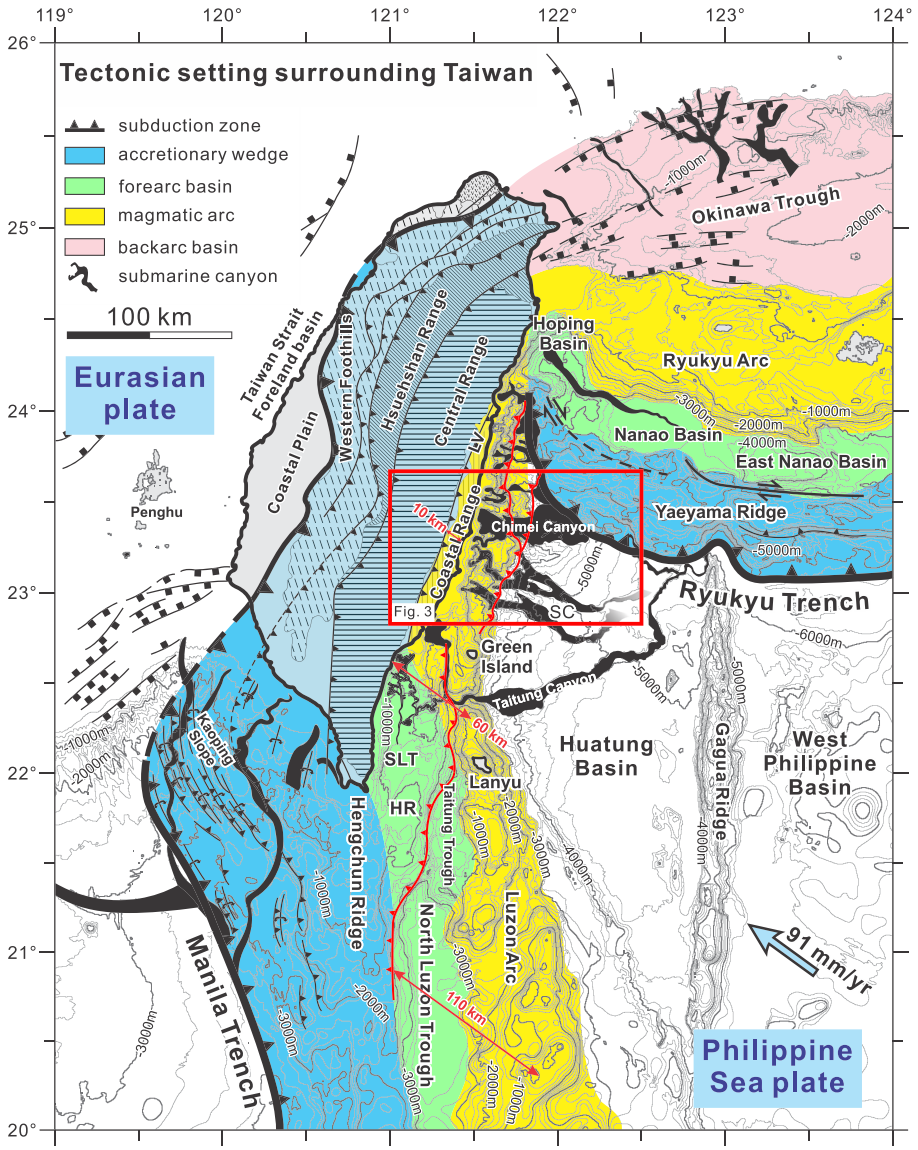

Figure 2. Tectonic setting of Taiwan, showing surrounding submarine canyons that currently transport orogenic sediment into deep ocean basins. The Taiwan arc-continent collision is located at the junction of two orthogonal subduction zones: The NS Manila subduction zone in the south extending to northern Taiwan and the EW Ryukyu subduction zone in the northeast, with associated Okinawa Trough backarc basin. The colors show tectonic elements (blue: accretionary wedge, green: forearc basin, yellow: magmatic arc, and red: backarc basin). SLT = Southern Longitudinal Trough; HR = Huatung Ridge; LV = Longitudinal Valley; SC=Sanxian Canyon. The offshore structures are from Liu et al. (2004) and submarine canyons from Chiang and Yu (2006), Hsiung and Yu (2011), and Yang (2001). The forearc basin is ~110 km wide in the south, measured in the plate convergence direction but is increasingly compressed northward during oblique arc-continent collision, becoming only ~10 km in the Taiwan Coastal Range.

et al., 1978; Chai, 1972; Ho, 1979, 1986; Suppe, 1981, 1984, 1987; Teng, 1990; Yu et al., 1997). This gives rise to a progressive southward propagation of the collision along the arc and southwestward along the continental margin (Suppe, 1981, 1984).

The Philippine Sea Plate is currently moving northwestward (~300° azimuth) with respect to the Eurasian Plate at a convergence of ~91 mm/yr, with a slower EW component of convergence (~30 mm/yr) prior to ~2 Ma (Kreemer et al., 2014; Seno et al., 1993; Tsai et al., 2015; Wu et al., 2016). This plate convergence is consumed in two orthogonal subduction systems with opposite polarity (Suppe, 1984). From Taiwan southward, the Eurasian Plate subducts beneath the Philippine Sea Plate along the Manila Trench and the western foothills, which form an accretionary wedge (Taiwan mountain belt to the north and its submarine

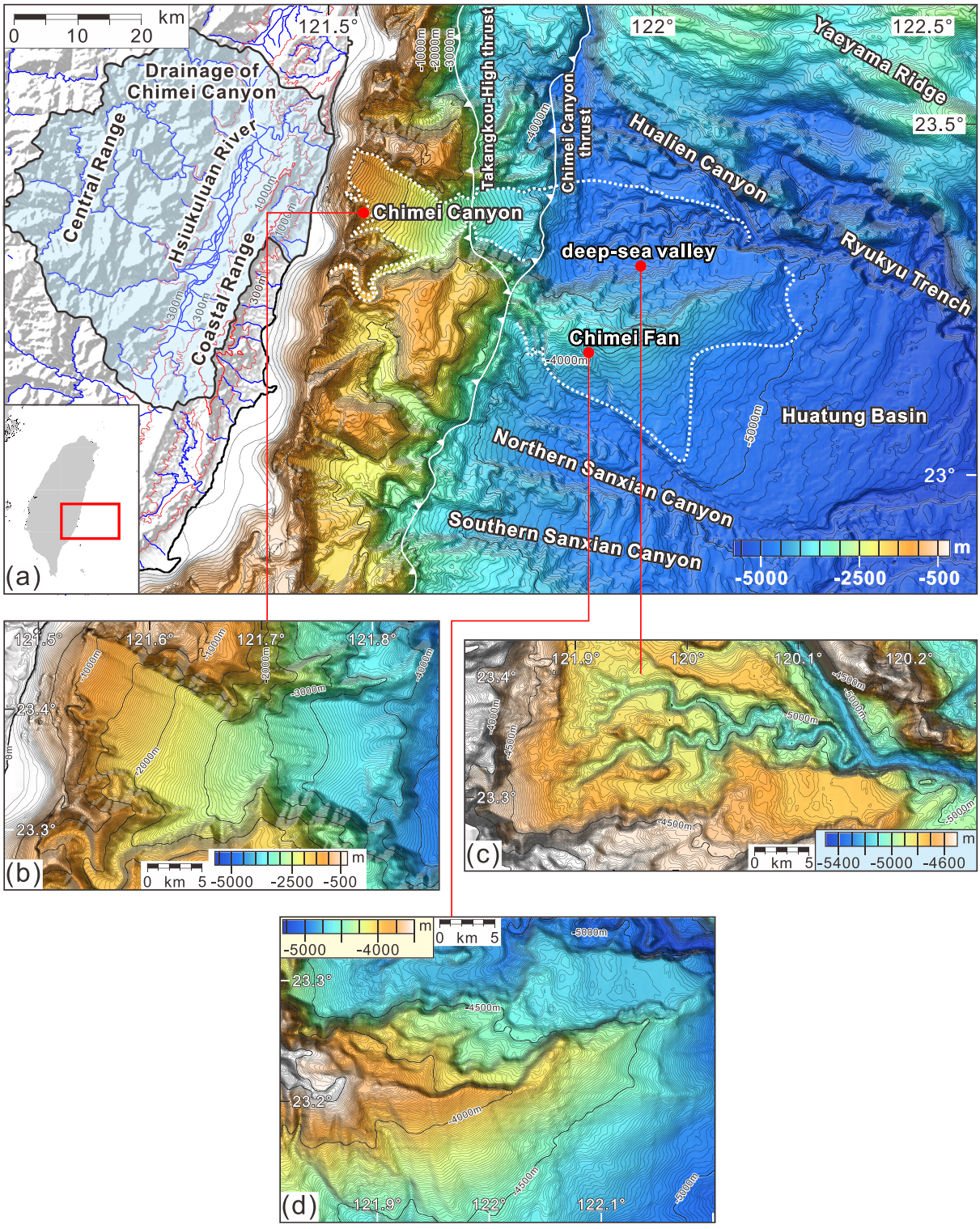

Figure 3. Detailed bathymetric map of the Chimei Canyon-Fan system (see location in Figure 2). Note that the depth range of the color scale is compressed in (c) and (d) to illuminate the low-relief deep-water morphologies. (a) Overview of the Chimei Canyon-Fan system. The outline of the canyon and fan is shown with white dots. The Chimei Canyon thrust lies at the foot of the slope, separating the canyon and deep-sea valley. The Takangkou High thrust cuts across the middle of the Chimei Canyon. Rivers onshore are shown by light blue lines and the Hsiukuluan River catchment (source of the Chimei Canyon-Fan system) is shown by light blue area. (b) Detailed bathymetric map of the Chimei Canyon showing a wide and smooth canyon bottom. (c) Detailed bathymetric map of the Chimei deep-sea valley. (d) Detailed bathymetric map of the Chimei Fan which shows the preserved southern part of the fan and erosional features in the northern part of the fan.

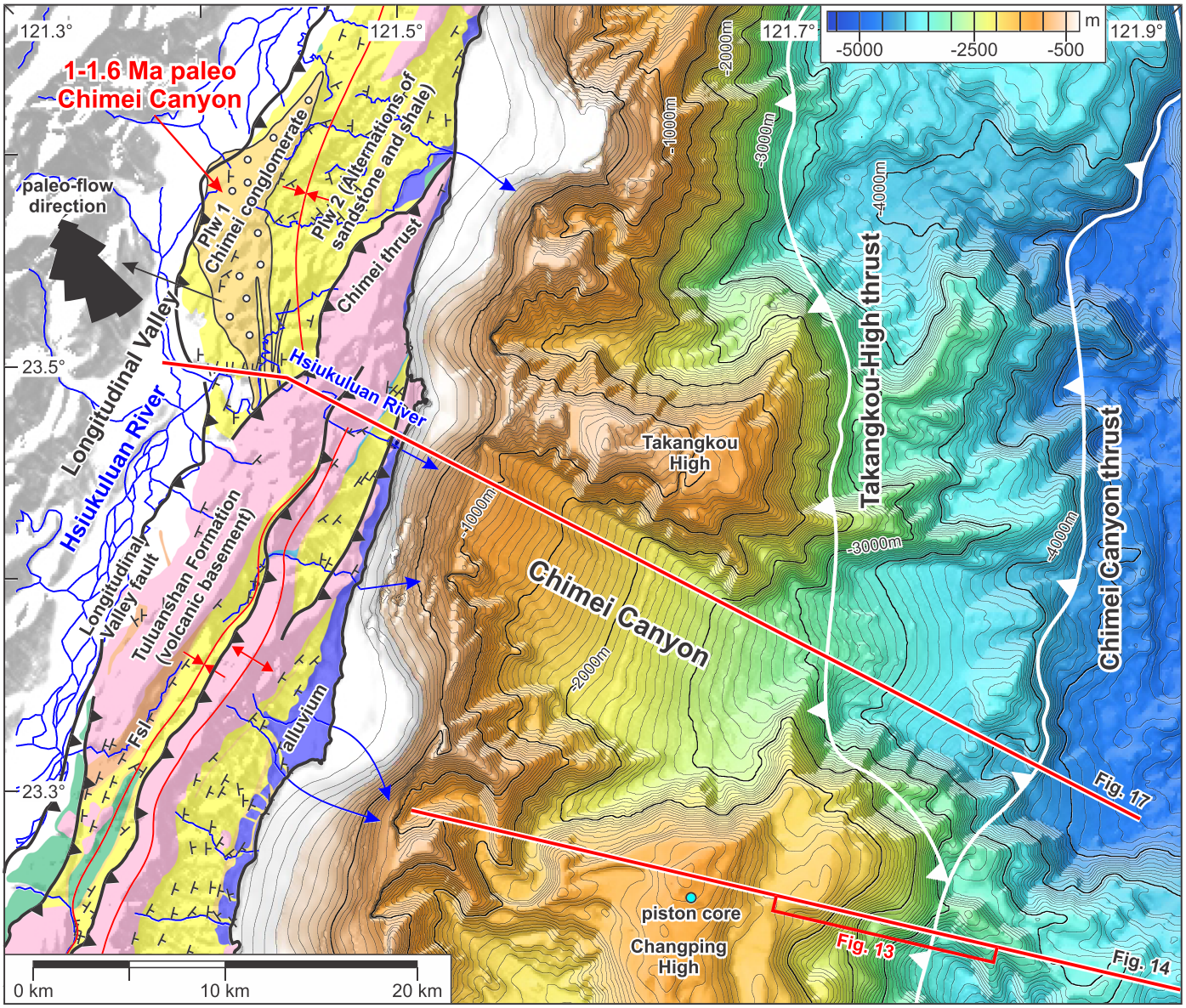

Figure 4. Combined geological map of the Coastal Range and bathymetric map offshore eastern Taiwan. The thin-skinned west-vergent Coastal Range thrust belt deforms arc and forearc basin strata, including paleo-submarine canyon and fan strata (Fanshuliao [Fsl] and Paliwan Formation [Plw1 and Plw2]) together with Luzon Arc (Tuluanshan Formation) uplifted to 1,000- to 1,500-m elevation, whereas the offshore Chimei Canyon has undergone east-vergent thrust deformation. The 1- to 1.6-Ma Chimei conglomerate exposed onshore is interpreted as a paleo-Chimei Canyon deposit, which shows a similar paleo-flow direction to the present-day upper Chimei Canyon (Dorsey & Lundberg, 1988). A cross section along the current transport pathway is shown as Figure 17. The geological map of Coastal Range is based on data from Wang and Chen (1993) and Shyu et al. (2006).

equivalents to the south: the Hengchun Ridge and Kaoping Slope), forearc basin (North Luzon Trough), and the Luzon Arc (Figure 2) (Bowin et al., 1978; Hayes & Lewis, 1984; Huang et al., 1992, 1997, 2006; Liu et al., 1992, 1997a; Reed et al., 1992; Suppe, 1981, 1984). Conversely, offshore of northeastern Taiwan, the Philippine Sea Plate subducts beneath the Eurasian continental margin along the Ryukyu Trench, which formed the Yaeyama Ridge (accretionary wedge), the Ryukyu Arc, and the Okinawa Trough back-arc basin (Font et al., 2001; Liu et al., 1997b; Park et al., 1998; Wang et al., 2004).

It is remarkable that about two thirds (~60 mm/yr) of the total ~90 mm/yr of plate convergence in Taiwan is consumed by deformation of the Luzon Trough forearc basin, Luzon Arc, and adjacent Huatung Basin of the Philippine Sea Plate, forming the East Taiwan thrust belt, which is composed of the Coastal Range thrust belt and the Offshore East Taiwan thrust belt. South of Taiwan, the forearc basin, has an undeformed width of about

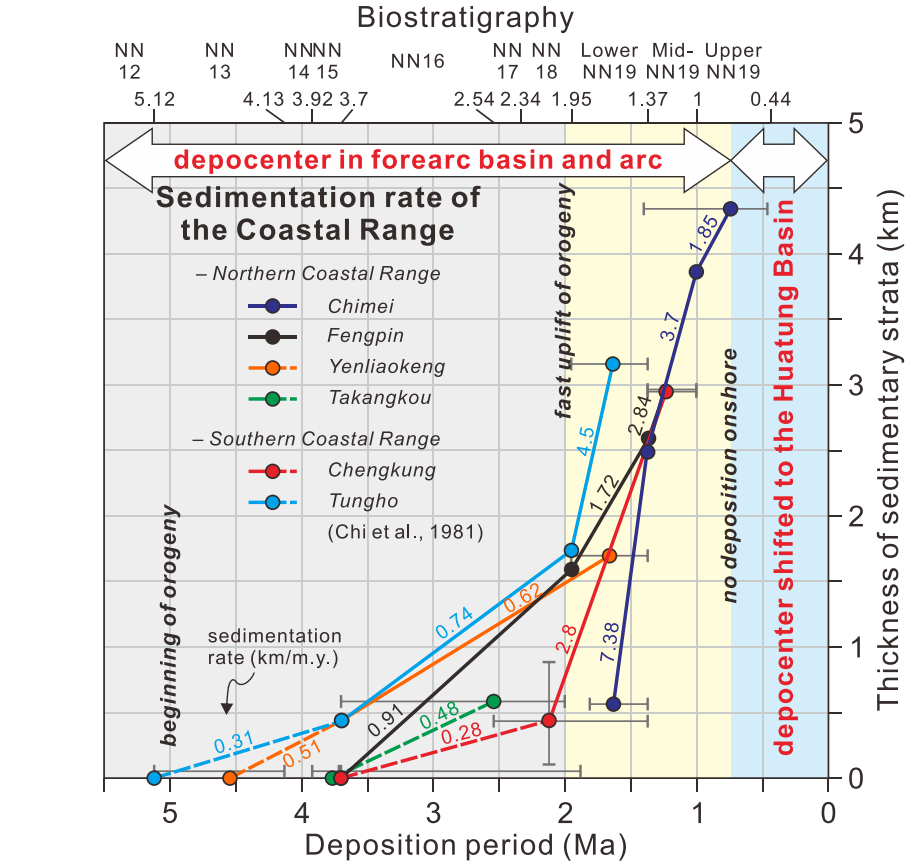

Figure 5. The sedimentation rate for stratigraphic sections of the Coastal Range (updated from Chi et al., 1981, using timescale of Cohen & Gibbard, 2019). The sedimentation rates increase abruptly around 2 Ma and sedimentation terminates ≲1 Ma. Different outcrop sections are shown by different colors. Values along each line show the average sedimentation rate in km/my. Gray lines are the error bars for age.

100–125 km but becomes progressively shortened northwards (Figure 2) to become the 10- to 15-km-wide Coastal Range thrust belt, which is strongly deformed and rapidly uplifting (5–10 mm/yr), reaching 1,000- to 1,500-m elevations in steeply dipping thrust sheets of Miocene arc volcanic rocks (Figure 4) (Chi et al., 1981; Hsieh et al., 2004; Hsieh & Rau, 2009; Liew et al., 1993). The lower elevations of the Coastal Range are underlain by more erodible thick sections of Plio-Pleistocene (1–4 Ma) Taiwan-derived flysch forearc-basin strata that overlie the arc volcanic rocks and generally show southeastward transport from the coeval Taiwan mountains to the north and west (Figure 4), similar to the current forearc basin offshore of southeastern Taiwan (Figure 2). These Taiwan-derived strata of the Coastal Range are important in the present context because they lie along the transport path of the source-to-sink system and are considered more proximal and in part older equivalents of the Chimei submarine canyon and fan deposits offshore, as discussed later (Figures 4 and 5).

An east-vergent thrust belt is observed offshore, east of the Coastal Range, based on multibeam bathymetry and multichannel seismic reflection data, here called the Offshore East Taiwan thrust belt. About ~2 cm/yr of convergence is currently consumed in the offshore based on published GPS data (Yu et al., 1997). The active Chimei Canyon thrust is the frontal thrust, which is marked by a sinuous bathymetric lineation at the foot of the slope offshore of the Coastal Range (Figure 3). It displays a fault scarp that is especially

clear at the foot of the Chimei Canyon (Figure 4) and separates the Chimei Canyon from the Chimei Fan. The Offshore East Taiwan thrust belt has been described based on multibeam bathymetry by Malavieille et al. (2002). In our present study, we use new prestack depth migration of the legacy seismic reflection data to better image the east-vergent thrust system, which underlies the Chimei Canyon and proximal fan.

The morphology of the proximal offshore eastern Taiwan reveals a narrow shelf, a steep slope, and several submarine canyons (Figure 3). In addition to thrust belt deformation, there are frequent earthquakes, strong climate effects, and submarine erosional processes (such as slides, slumps, and turbidity currents) that play important roles for shaping the morphology offshore eastern Taiwan (Lallemand et al., 2016; Lehu et al., 2015, 2016).

2.2. Stratigraphic Setting of Onshore and Offshore Eastern Taiwan

The source-to-sink pathway from the eroding Taiwan Central Range to the Chimei Canyon and Fan depocenter traverses the rapidly uplifting 10- to 15-km-wide Coastal Range, which extends for ~140 km along the east coast of Taiwan, forming a topographic barrier that is currently only breached by the Hsiukuluan River gorge that feeds the Chimei Canyon (Figures 3a and 4). The Coastal Range is essential to understanding the development of the offshore Chimei Canyon and Fan because it provides a more proximal stratigraphic record on the Philippine Sea Plate of the subduction to collision transition (Chi et al., 1981). The Coastal Range stratigraphy records the main locus of arc and forearc basin orogenic deposition in the Pliocene and early Pleistocene, prior to the shift of depocenter exclusively to the Huatung Basin east of the Luzon Arc after ~1 Ma (Figure 5). The sediment of the Chimei Canyon-Fan may be considered the distal and in part younger equivalents of strata in the Coastal Range.

The exposed stratigraphic record in the Coastal Range thrust belt shows a Miocene volcanic arc and volcaniclastic sequence (Tuluanshan Formation) with local development of overlying Pliocene shallow-water carbonates (Kangkou Limestone) and a regionally onlapping very thick Plio-Pleistocene clastic sequence that is dominantly composed of Taiwan-derived orogenic sediments (Chen, 2016; Huang et al., 2018; Wang & Chen, 1993), but also contains minor interbedded arc-derived sediments and tuffs (e.g., Chi et al., 1981; Dorsey, 1985, 1988; Lai et al., 2018). The base of the Plio-Pleistocene orogenic clastic sequence is time transgressive, filling forearc basin and onlapping and overlapping arc bathymetry (Dorsey, 1992; Lai et al., 2018; Wang & Chen, 1993). The early Pliocene to lower Pleistocene Fanshuliao Formation shows mudstone alternating with sandstone or shale. This sequence is interpreted as turbidites deposited in the forearc basin with a low sedimentation rate. The Fanshuliao Formation shows both arc-derived and Taiwan-derived petrographies (Chi et al., 1981; Dorsey, 1988; Teng, 1979). The upper sequence, called the Paliwan Formation, consists of sandstone alternating with shale, which is interpreted as turbidites and tempestites deposited in the forearc basin from the lower Pleistocene to ~0.8 Ma with a high sedimentation rate (Chen, 2016; Chi et al., 1981; Dorsey & Lundberg, 1988; Ho, 1969; Huang et al., 2018; Teng, 1990; Wang & Yang, 1974). In the section just north of the Hsiukuluan River, the Paliwan Formation contains a massive 15-km-wide and 2-km-thick lens of cobble-boulder conglomerate and thick bedded graded sandstones, location shown in Figure 4, that is interpreted as a proximal submarine canyon deposit that may record an early stage (1.6–1 Ma) of the present Hsiukuluan River-Chimei Canyon source-to-sink pathway (Dorsey & Lundberg, 1988, 1989).

The denudational and depositional record in the Central and Coastal Ranges can be divided into two stages of Taiwan arc-continent collision (Figure 5). In the first stage from 2–5 Ma, collisional mountain building was initiated; uplift and exhumation in the Central Range were relatively slow based on thermochronology (0.65–1.74 mm/yr; Byrne et al., 2011 ; Hsu et al., 2016), and the sedimentation rate of Taiwan-derived strata in the Coastal Range is a modest 0.28–0.91 km/my (Chi et al., 1981). The second stage began about 2 Ma, uplift and exhumation in the Central Range accelerated to ~ 2.45–10 mm/yr (Byrne et al., 2011; Hsu et al., 2016), and sedimentation rate in the Coastal Range increases to 1.72–7.83 km/my (Chi et al., 1981) (Figure 5).

In contrast with the relatively well-dated onshore record, the ages of the offshore seismic stratigraphy are not calibrated because of the absence of a drilling in the basin. Nevertheless, we can make indirect estimates of their ages based on regional source-to-sink considerations as described in the discussion section. Most obviously, the deformation and uplift of the Coastal Range depocenters has necessarily shifted the locus of late Pleistocene (<1 Ma) deposition completely to the Huatung Basin east of the Luzon Arc (Figure 5).

In addition, we note the existence of a 4-m-long piston core (KR03) collected on the Changping High on the southern flank of Chimei Canyon (Figures 4 and 6), which shows olive-gray clay hemipelagites with a

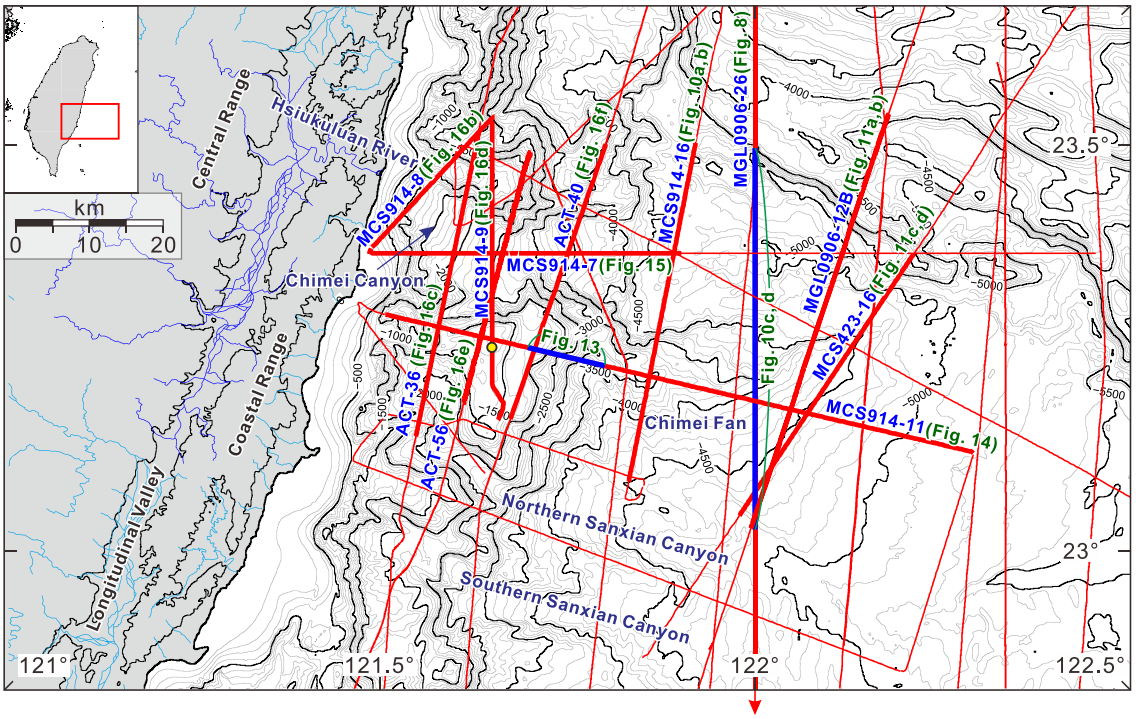

Figure 6. Location map showing the seismic reflection profiles used in this study. Bold lines are the seismic profiles shown in this paper. Yellow dot is the location of the marine core (Lallemand et al., 2016; Lehu et al., 2016).

depositional rate approximate of 1.09 mm/yr. The 4 m of cored sediment were deposited since ~1,673 BC (Lallemand et al., 2016).

3. Data and Processing

Both high-resolution bathymetric data (100-m grid) and multichannel seismic reflection data are used to study the Chimei Canyon-Fan system. The high-resolution swath bathymetry data were acquired during the ACT cruise in 1996; more description of the seafloor morphology is shown in Lallemand et al. (1997), Liu et al. (1998), and Malavieille et al. (2002).

The multichannel seismic reflection data we analyzed were collected from several cruises, including OR1-423, OR1-914, ACT, EW9509 (the TAICRUST project), and MGL0906 (the TAIGER project). Table 1 shows detailed information on those multichannel seismic reflection acquisitions. Figure 6 shows the locations of

Table 1
Acquisition Parameters for Multichannel Seismic Reflection Data Used in This Study

		Streamer parameters				Source parameters			Recording parameters		
Cruises	Line	Shot interval	Channels	Channel interval	Streamer length	Source	Source volume	Source pressure	Record length	Sample rate	Data source
OR1-914	7, 8, 9, 10, 11, 12, 13, 15, 16	50 m	84	12.5 m	1,037.5 m	Airgun	775 in^3	200 bar	10 s	2 ms	MOST, Taiwan
MGL0906	12B, 26, 26A, 30A	50–75 m	468	12.5 m	5,837.5 m	Airgun 40 guns	6,600 in^3	2,000 psi	15 s	2 ms	TAIGER, Taiwan/USA
EW9509	5, 7	50 m	160	25 m	3,975 m	Airgun 20 guns	8,470 in^3	2,000 psi	16 s	2 ms	TAICRUST, Taiwan/USA
OR1-423	16	43 m	56	25 m	1,375 m	Airgun	700 in^3	200 bar	10 s	4 ms	MOST, Taiwan
ACT	36, 40, 55, 56, 61, 71, 72, 73	50 m	6	50 m	250 m	GI gun	150 in^3	155 bar	6 s	4 ms	ACT, Taiwan/France

the seismic reflection profiles used in this study. Seven high-resolution seismic profile images are provided in the Supporting Information S1, including five poststack time migration seismic profiles and two prestack depth migration profiles (Figures S1–S7).

Most seismic data were processed at the Seismic Exploration Lab, Institute of Oceanography, National Taiwan University. ProMAX seismic data processing software was used to obtain poststack time-migrated profiles, whereas two E-W trending legacy short-streamer seismic profile data were reprocessed using ECHOS and GeoDepth seismic data processing software to obtain improved prestack depth-migrated profiles that help constrain the structure of the Offshore East Taiwan thrust belt.

4. Morphology

The Chimei Canyon-Fan system shows a distinct morphology that can be divided into two parts: a submarine canyon and a deep-sea fan complex. The deep-sea fan complex can be further subdivided into two parts: a complex deep-sea valley that starts at the foot of the canyon (Figure 3c) and a submarine fan that is preserved along the south side of the deep-sea valley (Figure 3d); the northern submarine fan has been largely eroded away (Figure 3). The canyon is confined to the region of the Offshore East Taiwan thrust belt (Figure 3a) and is flanked by uplifted and deformed western Chimei Fan strata that underlie the Changping High to the south and the Takangkou High to the north (Figure 4), which are imaged in seismic reflection profiles (see section 6). The eastern part of the Chimei Fan east of the frontal Chimei Canyon thrust has not been involved in compressional Taiwan arc-continent collision.

In the following sections, we utilize a slope map of the Chimei Canyon-Fan system (Figure 7) that was computed in ArcGIS based on 100-m high-resolution bathymetric data. This map shows a smooth Chimei Canyon floor that is truncated downstream by the surface break of the frontal Chimei Canyon thrust, below which the transport pathway becomes a deep-sea meander (compare Figures 3 and 7).

4.1. The Chimei Canyon

The Chimei submarine canyon starts just offshore of the Hsiukuluan River mouth on the eastern flank of the Coastal Range and ends ~40 km to the east at the Chimei Canyon thrust, which is the frontal thrust of the east-vergent thrust belt (Figures 3, 4, and 7). The canyon displays a broad flat-bottomed U-shape (box shape) in cross section with a smooth-bottom width of ~5–14 km (Figures 1, 3, 4, and 7a–7d). The Chimei Canyon head starts with an abrupt 900-m drop from sea level in ~3 km (~20° slope) from the Hsiukuluan River mouth to the point at which a flat-bottomed U-shape morphology is observed and is maintained until its distal end (Figure 7b). The smooth Chimei Canyon floor has a constant slope gradient ~5 $\pm$ 1° (Figures 7c and 7d). The canyon bottom widens from the head (~5 km wide) to the middle part of the canyon (~14 km wide), then narrows to ~5 km due to active thrusts that run across the middle part of the canyon (Figures 3, 4, and 7b). The average height of the canyon wall is 950 m, and the maximum height is 1,455 m. The characteristics of the Chimei submarine canyon thalweg are also distinct from the deep-sea valley (Figures 7c–7e).

The morphology of the Chimei Canyon has been affected by active structures, including the Takangkou High thrust and the Chimei Canyon frontal thrust, which cut through the middle and at the foot of the canyon, respectively (Figure 7c). The Takangkou High thrust runs along the eastern edge of the Takangkou High and cuts through the Chimei Canyon in the middle and merges into the Chimei-Canyon frontal thrust near the Changping High south of the Chimei Canyon (Figure 4). The Takangkou High thrust does not show a distinct fault-scarp morphology on the canyon floor in contrast with the Chimei Canyon frontal thrust suggesting it is currently less active relative to the presumed high rate of erosional and depositional surface processes of the active canyon bottom. Nevertheless, the Takangkou High thrust is associated with distinct morphologic changes, including steeper and variable canyon gradients (Figure 7d), the incision of secondary channels on the hanging wall (Figure 3b), changes in canyon width and wall height (Figure 7e), and a deflection of Chimei Canyon axis from northwest-southeast to east-west. The Takangkou High thrust shows folding of hanging wall growth strata at shallow depth imaged by seismic reflection (see section 6.1). The Chimei Canyon frontal thrust has formed a pronounced bathymetric scarp at the foot of the Chimei Canyon, which separates the Chimei Canyon from the Chimei Fan and is morphologically associated with secondary channels in the hanging wall (Figures 3b and 4) and steeper gradients (Figure 7d). The Chimei Canyon morphology ends at the foot of the slope (Figure 4).

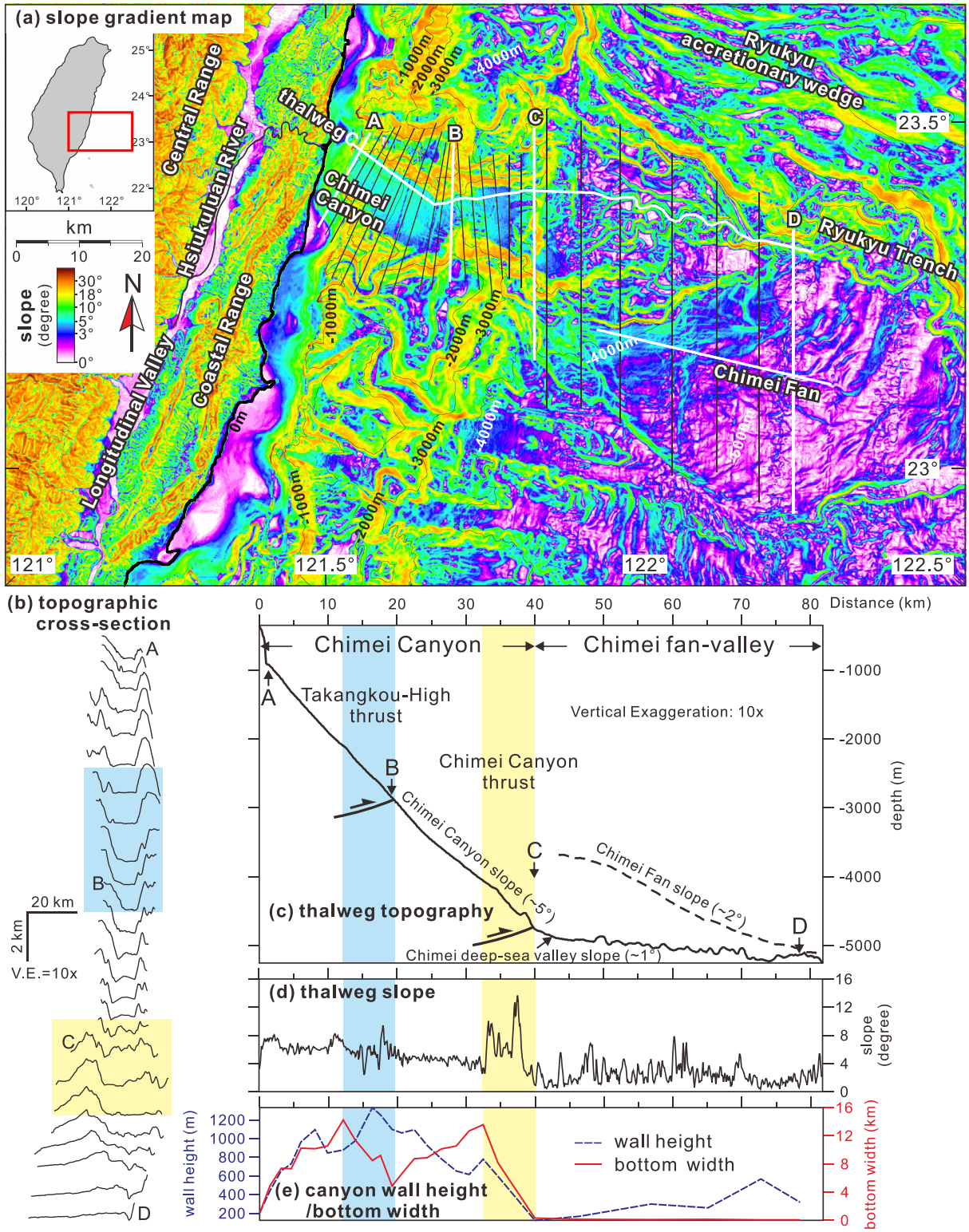

Figure 7. (a) Slope gradient map of the Chimei Canyon-Fan system. (b) Topographic cross sections of the Chimei Canyon-Fan system from upstream to downstream. The locations of cross-sections are shown in (a), with four profiles marked by A–D. (c) Canyon, deep-sea channel thalweg, and fan topography. (d) Slope gradient along the Chimei Canyon and deep-sea channel thalweg. (e) Height of the canyon/deep-sea channel walls and width of the canyon/deep-sea channel bottom. Two active thrust zones with associated folding are shown by blue and yellow background.

The Chimei Canyon is currently asymmetric, with a steeper canyon wall on the north side and an adjacent active channel that may connect to the Hsiukuluan River. On the south side, two tributaries merge into the Chimei Canyon, with more gentle and incised canyon walls (Figure 4). The fact that the Huatung Basin lithosphere is bending northward as it is subducted along the Ryukyu Trench may cause the north-wall channel to be pinned along the steeper north canyon wall, leading to a progressive widening of the Chimei Canyon by a process analogous to the channel pinning of *downstream sweep erosion* recently documented subaerially in western Taiwan (Cook et al., 2014).

4.2. The Chimei Fan Complex

The Chimei Fan complex includes a deep-sea valley in the northern part of the complex and a submarine fan in the southern part of the complex. The deep-sea valley includes dendritic deep-sea channel and associated levees. The western part of the Chimei Fan has been uplifted as the Offshore East Taiwan thrust belt.

The Chimei Fan is an asymmetrical fan with essentially all of the presently preserved fan morphology occurring south of the Chimei deep-sea valley (Figure 3). We suggest that the Chimei Fan was originally symmetrical, but the northern part of the fan has been largely eroded away and a dendritic deep-sea channel developed later. Possible remnants of this northern fan exist as the ridge separating the Chimei deep-sea valley and the Hualien Canyon, based on seismic facies imaged in the NS seismic profiles (see section 5.3; MCS914-16, MGL0906-26A, Figure 10).

The Chimei Fan can be divided into an upper and a lower fan based on morphological characteristics. The upper fan (proximal fan) is identified by a large-scale deep-sea valley with pronounced levees which show concave-upward levee topography, whereas the lower fan (distal fan) is identified by smaller channels and levees which have flat and convex-upward levee topography, merging gradually into the surrounding basin plain (Mitchum, 1985). The Chimei Fan is between 3,200 and 5,000 m deep. Its length along the main deep-sea channel is 43–57 km, and its width across the main deep-sea channel is approximately 33–45 km. The thickness of the fan is 2 km. The Chimei Fan covers an area of approximately 1,200–2,087 km^2. The area of the fan is estimated to be 1,200 km^2 based on the slope gradient of bathymetry, but facies identification within the seismic data defines the area of influence of the fan to be larger (2,087 km^2). The size of the fan defined by seismic facies is larger than that defined by seafloor morphology probably because it is hard to recognize morphological characteristics of the lower fan (Mitchum, 1985). Generally, the lower fan is characterized by very little local relief, merging into the surrounding basin plain gradually.

The dendritic deep-sea channels are developed in the Chimei Valley (Figure 3c), which functions as the downstream continuation of the Chimei Canyon. The average slope gradient of the channels is 1–3°. The dendritic channels have a wide bottom (~300 m) and shallow incision (~125 m) at the head of dendritic deep-sea channels, and the dendritic deep-sea channels merge into a larger main channel downstream with a narrow bottom width (100 m) and deeper incision (300 m) (Figures 7b and 7e). The deep-sea channels finally merge into the Hualien Canyon near the western end of the Ryukyu Trench offshore eastern Taiwan. We suggest that the dendritic deep-sea channels in the Chimei deep-sea valley may transport sediments out from the Chimei Canyon-Fan system.

5. Seismic Stratigraphy

5.1. Seismic Sequences

We have identified three seismic sequences in the sedimentary strata of our study area based on truncation, toplap, and baselap of reflection signals (Mitchum & Vail, 1977; Mitchum, Vail, & Sangree, 1977; Mitchum, Vail, & Thompson, 1977). The three seismic sequences are separated by two seismic sequence boundaries *X* and *Y*, which were defined by Liu et al. (1997a), Malavieille et al. (1997), Schnürle et al. (1998), Yang (2001), and Hung (2010). The seismic sequence boundaries *X* and *Y* are Huatung Basin-wide boundaries (Liu et al., 1997a) and have significant implications for the depositional history of the Huatung Basin which is closely linked to Taiwan arc-continent collision (Figure 8).

1. *Lower seismic sequence*. Lower seismic sequence sits on top of the Huatung Basin basement and below sequence boundary *Y*. Reflections in this sequence are generally parallel, concordant and continuous, and locally onlap relief of the Huatung Basin oceanic basement.

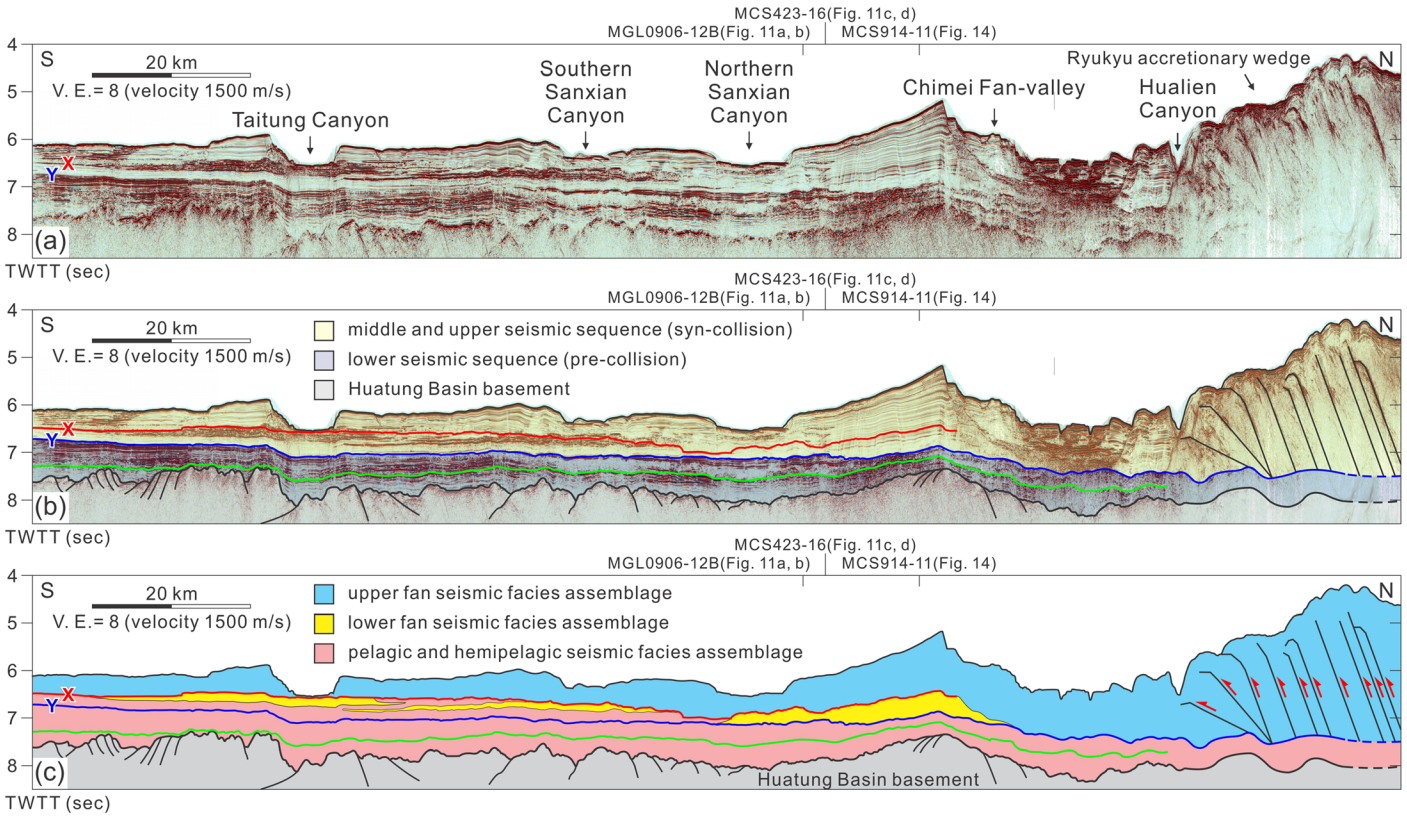

Figure 8. Three seismic sequences in the Huatung Basin. (a) The NS seismic profile MGL0906-26 in the northern Huatung Basin. (b) Seismic interpretation (see Figure S1 for high-resolution versions of this profile, with seismic facies). Three seismic sequences with two seismic sequence boundaries (*X* and *Y*) are shown. The lower seismic sequence, which represents the pre-collisional sequence, is shown by purple color. The middle and upper seismic sequences, which represent syn-collisional sequences, are shown by yellow color. (c) Main seismic facies in seismic sequences. Pink, yellow, and blue show pelagic and hemipelagic, lower fan, and upper fan seismic facies, respectively. Submarine fan seismic facies propagates to south within the middle sequence, which is consistent with progressive propagation of the oblique arc-continent collision southward. Tick marks at the top with seismic-profile names and figure numbers show the intersection of crossing seismic profiles in this paper.

2. *Middle seismic sequence*. Reflections above seismic sequence boundary *Y* reveal downlap on the seismic sequence boundary *Y* in the northwest Huatung Basin. Reflections in this seismic sequence are more transparent and have more seismic facies changes than reflections in the lower seismic sequence.
3. *Upper seismic sequence*. The upper seismic sequence extends from seismic sequence boundary *X* to the seafloor. Reflections of the upper seismic sequence reveal onlap on top of the middle seismic sequence (on sequence boundary *X*) along the eastern flank of the Luzon Arc. Reflections in the upper seismic sequence are continuous but wavy and transparent.

5.2. Seismic Facies

We have identified six seismic facies (Figure 9) on seismic profiles. Our classification of seismic facies is modified from the seismic interpretation of classic depositional facies by Sangree and Widmier (1977). In the following paragraphs, we first describe characteristics of each seismic facies and then describe the distribution of seismic facies in each seismic sequence to understand the depositional environment changes from the lower to upper seismic sequences and the evolution of the Chimei Canyon-Fan system through time.

Seismic facies 1: Basinal widespread sheet-drape seismic facies (Huatung Basin seismic facies) (Figure 9).

This seismic facies is characterized by widespread, parallel, or subparallel reflection configurations. Reflections show concordant pattern and onlap on basement. Amplitudes vary from low amplitude at bottom to high amplitude at top. Continuity is high. This facies dominates the lower seismic sequence of the Huatung Basin.

Seismic facies	Seismic characteristics	Geological interpretation
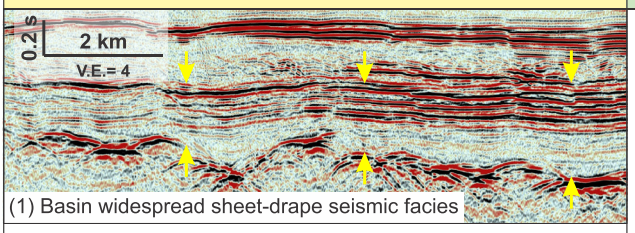	- Basinal widespread, parallel or subparallel reflection. - Reflections show concordant pattern and onlap on basement. - Amplitude varies from low amplitude at bottom to high amplitude at top.	Pelagic sediments (Higuchi et al., 2007; Plank et al., 2000).
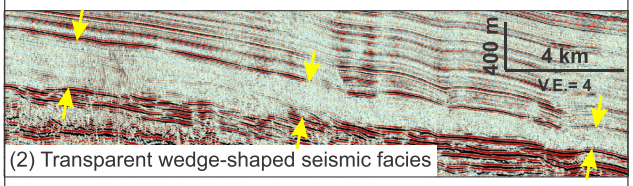	Low continuity, low-amplitude reflections that show downlap on seismic sequence boundary Y.	Overbank deposits in distal lobe complex in a submarine fan (Lopez, 2001; Normark et al., 1998; Schwenk et al., 2005).
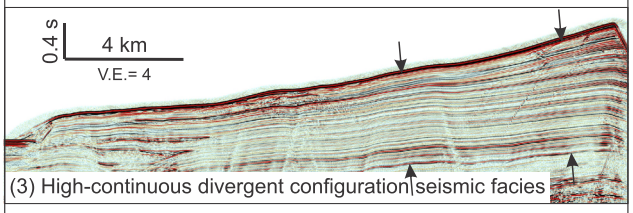	Very high-continuous, low to moderate-amplitude divergent reflections.	Submarine fan levee which is composed of deep-sea clay alternating with silty beds (Lallemand et al., 2016).
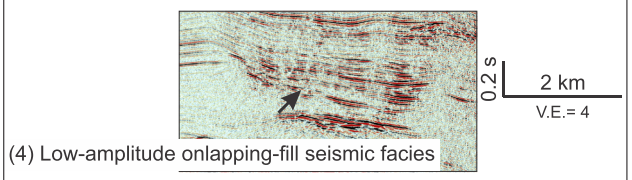	Continuous, low to moderate-amplitude parallel reflections onlap on V- or U-shape channel.	Buried channel (Schwenk et al., 2003; Schwenk et al., 2005).
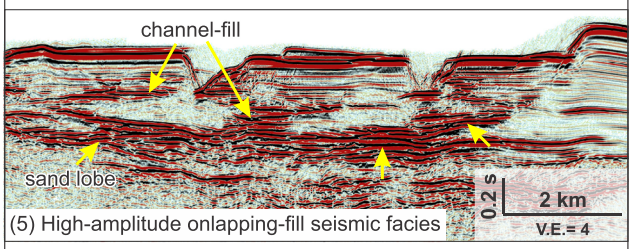	High-amplitude hummocky reflections.	Channel-fill in deep-sea channels (Lopez, 2001; Posamentier & Kolla, 2003) or sand lobes at the base of the slope (Schwenk et al., 2005).
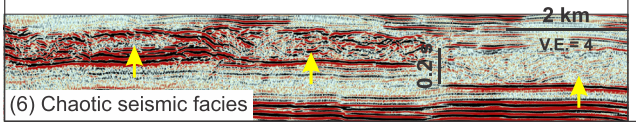	Low-to-high or variable-amplitude, poor- to low-continuity reflections with contorted and discordant internal pattern.	Mass-transport deposits, slumps, creeps, unconfined turbidites (Sangree & Widmier, 1977).

Figure 9. Main seismic facies identified in the study area. Seismic facies indicated by arrows.

We interpret seismic facies 1 as pelagic sediment of the Huatung Basin. Similar seismic facies has been shown in seismic reflection data in the northern Philippine Sea (e.g., Higuchi et al., 2007), and in ODP sites 801 and 1149 northwestern Pacific. The low-amplitude reflections are pelagic clay, and the high-amplitude reflections are interbedded radiolarian chert, porcellanite, and siliceous clay based on the OPD drilling (Plank et al., 2000).

Seismic facies 2: Transparent wedge-shaped seismic facies (Figure 9).

Seismic facies 2 is characterized by low-amplitude reflections that show downlap on seismic sequence boundary *Y*. Reflections sometime appear wavy. In seismic section parallel to the main channel, this

facies appears to be wedge-shaped tapering in down channel direction, whereas the facies becomes mound-shaped in the seismic section perpendicular to the main channel.

We interpret seismic facies 2 as channel levee/overbank deposits in the distal lobe complex. This interpretation corresponds well that in the Bengal Fan (Schwenk et al., 2005), Amazon Fan (Lopez, 2001), and Hueneme Fan (Normark et al., 1998), where the same seismic facies are observed. The more distal transparent equivalents of facies 2 in the middle sequence without downlap, far from Chimei Fan, show similarities to the transparent varieties of seismic facies 1 and may be hemipelagic (Figures 8 and S1).

Seismic facies 3: High-continuous divergent configuration seismic facies (also called levee seismic facies) (Figure 9).

This seismic facies is characterized by very high-continuous, low- to moderate-amplitude divergent reflections that cover paleotopography smoothly with only gradual changes in thickness or amplitude. In seismic sections parallel to the main channel, reflections are almost parallel. In seismic sections perpendicular to the main channel, reflections are divergent and thicken toward the main channel. This facies is fan-shaped in three-dimensions. Therefore, we interpret this seismic facies as submarine fan deposits.

We have also found this seismic facies in the Changping High and the Takangkou High, the two sidewalls of the Chimei submarine canyon. A gravity core collected on the top of the Changping High shows that the sediments are deep-sea clay hemipelagites alternating with silty beds (Lallemand et al., 2016), the type of sediments commonly found in a submarine fan.

Seismic facies 4: Low-amplitude onlapping-fill seismic facies (also called buried channel seismic facies) (Figure 9).

The seismic facies 4 is characterized by continuous, low to moderate-amplitude parallel reflections. It represents channel-fill sediments that onlap on V- or U-shape channel in seismic sections that are perpendicular to the main channel (Schwenk et al., 2003, 2005). This facies is usually interpreted as buried channel (Schwenk et al., 2005).

Seismic facies 5: Hummocky, high-amplitude onlapping-fill seismic facies (also called channel seismic facies) (Figure 9).

The seismic facies 5 is characterized by high-amplitude hummocky reflections. This seismic facies is confined in the Chimei deep-sea valley system which is at the base of the Chimei Canyon. This facies is interpreted as sand-rich turbidite channel-fill sediments in the deep-sea channels, or sand lobes at the base of the slope (Schwenk et al., 2005). Similar seismic facies also found deep-sea channel complex offshore Borneo, Kalimantan, Indonesia (Posamentier & Kolla, 2003), and Amazon Fan (Lopez, 2001).

Seismic facies 6: Chaotic seismic facies (Figure 9).

This seismic facies is characterized by an internal pattern of contorted and discordant reflections, also commonly shows diffractions. Chaotic seismic facies displays both low and high amplitudes, which may reflect different sedimentary materials. In the Huatung Basin, the seismic facies 6 usually appears elongated shape along the slope and appears mounded shape across the slope. Mass-transport deposits, slumps, creeps, or unconfined turbidites are thought to be responsible for the chaotic seismic facies (Sangree & Widmier, 1977).

5.3. Seismic Facies Distribution of the Chimei-Fan System

To understand the development of the Chimei Fan system and its relationship with Taiwan arc-continent collision, we present four seismic profiles from proximal fan (upper fan) to distal fan (lower fan) (Figures 10, 11, and S2–S5). We define the upper (proximal) and lower (distal) fans based on seismic facies assemblage. The seismic facies assemblage of the upper fan consists of one or a few thick, sand-prone channels (facies 4 or 5) flanked by large, mostly silt- or shale-prone levees (facies 2 or 3), whereas the seismic facies assemblage of the lower fan shows a convex-upward, bidirectional opposing downlap reflection pattern (facies 2 or 3) without channels (Mitchum, 1985). Lower fan also shows high-amplitude lenticular sand lobe (seismic facies 5 below Taitung and Southern Sanxian Canyons; Figure S1). We use the seismic assemblage of the upper/lower fan within middle and upper seismic sequences to describe the evolution of the Chimei Canyon-Fan system.

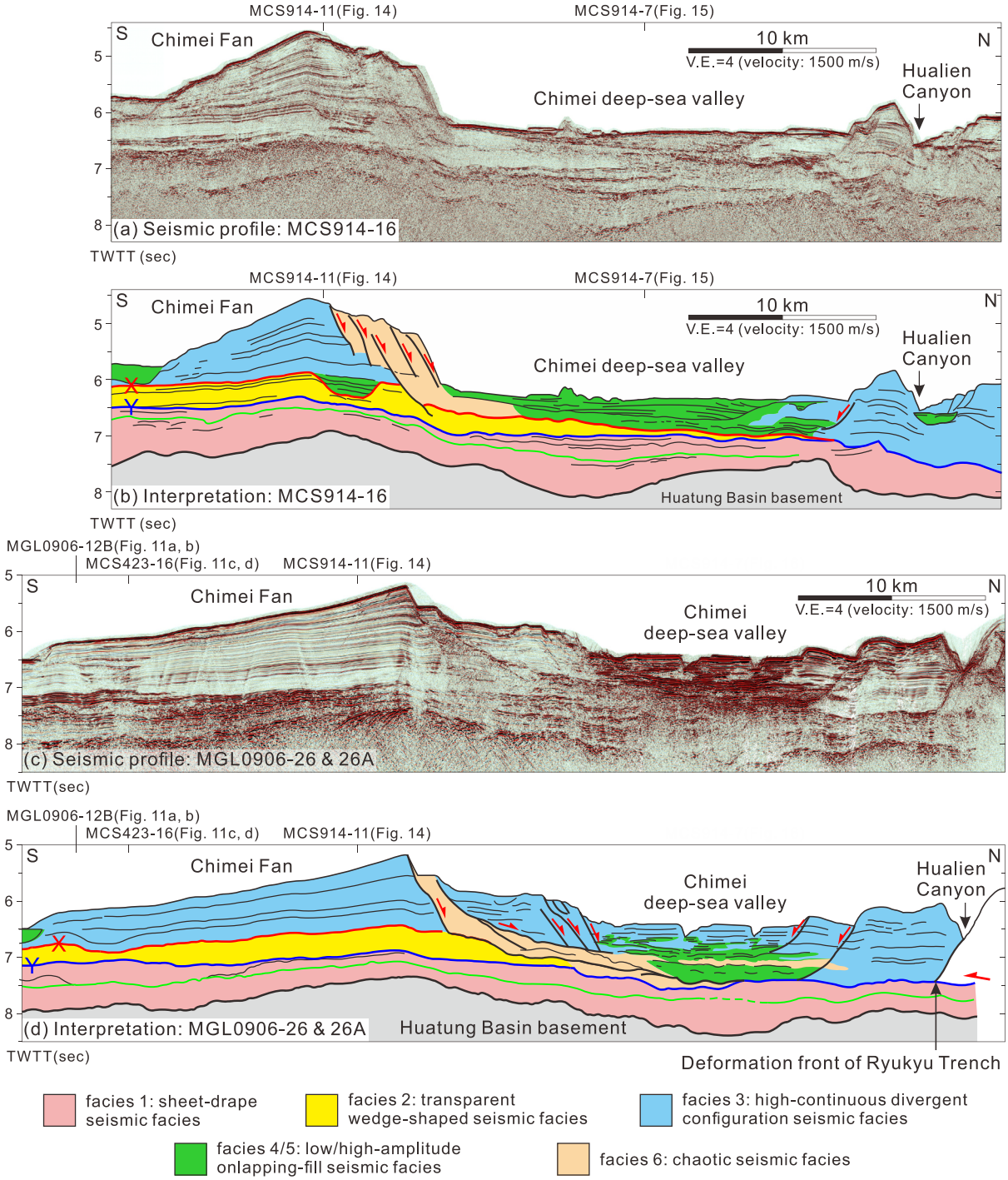

Figure 10. Upper fan seismic profiles of the Chimei Fan. (a) Seismic profile MCS914-16. This seismic profile is the closest profile to the canyon (see Figure 6 for location). (b) Seismic interpretation of (a). (c) Seismic profile MGL0906-26 and 26A. (d) Seismic interpretation of (c). *X* and *Y* are seismic sequence boundaries. Colors show the seismic facies. Locations of crossing seismic profiles are given by tick marks. See Figures S2 and S3 for high-resolution versions of those profiles.

5.3.1. Seismic Facies of the Lower Seismic Sequence

Within the lower seismic sequence, the basinal widespread sheet-drape seismic facies (seismic facies 1) is dominant. We can see that horizontal parallel/subparallel reflections of this seismic facies show onlap on the Huatung Basin oceanic basement (Figures 8, 10, 11, and S1–S3). We also find some chaotic seismic

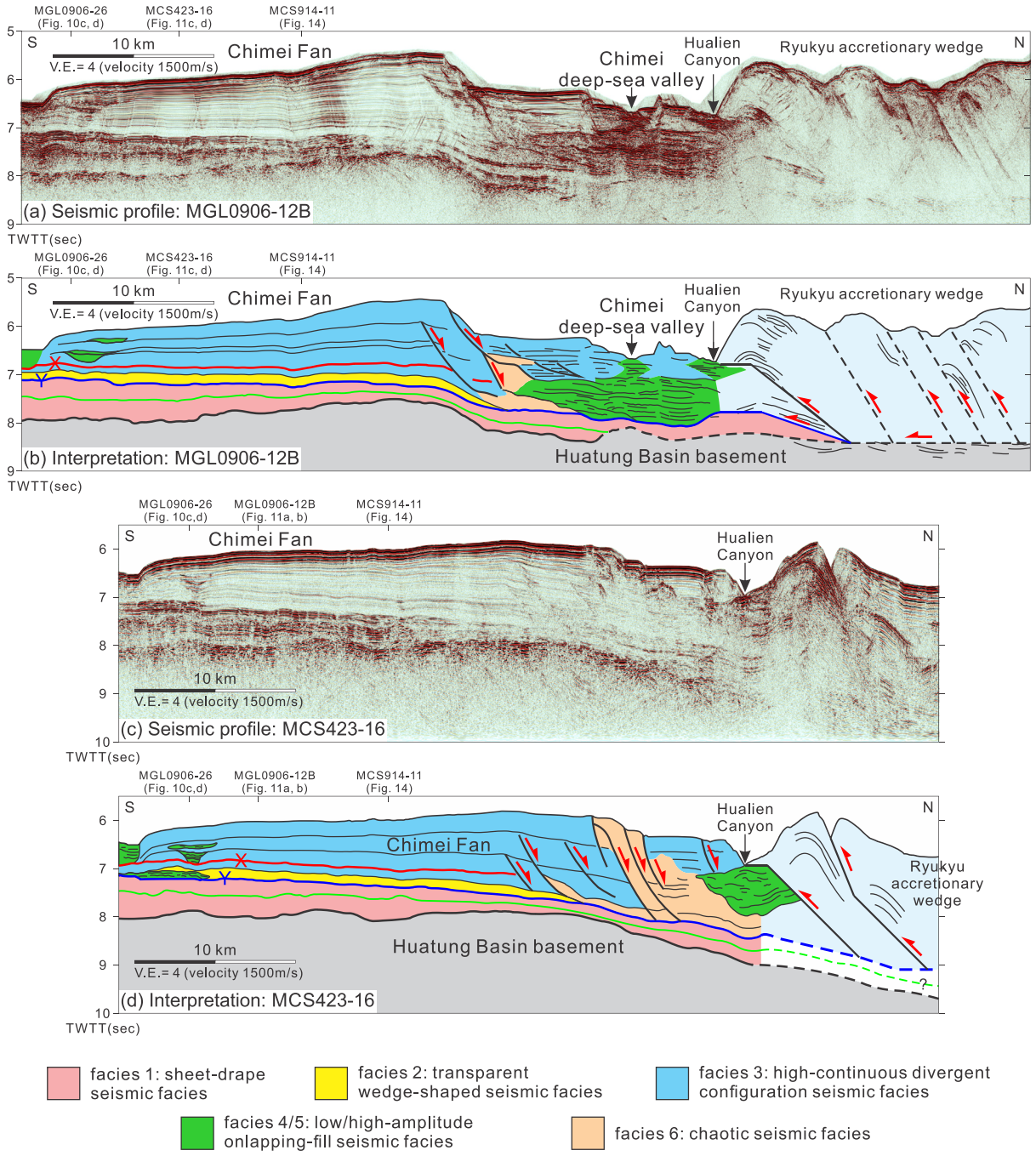

Figure 11. (a) Seismic profile of the Chimei fan and deep-sea valley: MGL0906-12B. This seismic profile shows that the Chimei Fan and deep-sea valley are beginning to be incorporated into the Ryukyu accretionary wedge. (b) Seismic interpretation of (a). (c) Lower fan seismic profile of the Chimei Fan: MCS423-16. This seismic profile is the easternmost profile across the Chimei Fan (see Figure 6 for location). The canyon in this profile is the Hualien Canyon because the Chimei deep-sea channels merged into the Hualien Canyon west of this seismic profile. See Figures S4 and S5 for high-resolution versions of these profiles.

facies 6 (turbidites and mass transport complex) interbedded with the sheet-drape seismic facies (seismic facies 1) in the upper part of the lower seismic sequence (e.g., Figures S1 and S6). The chaotic seismic facies becomes more developed toward the Luzon Arc and may reflect the distal input from the Luzon Arc after it was established ~15 Ma. The seismic facies assemblage is commonly found in the low-energy deep-marine environment (Sangree & Widmier, 1977).

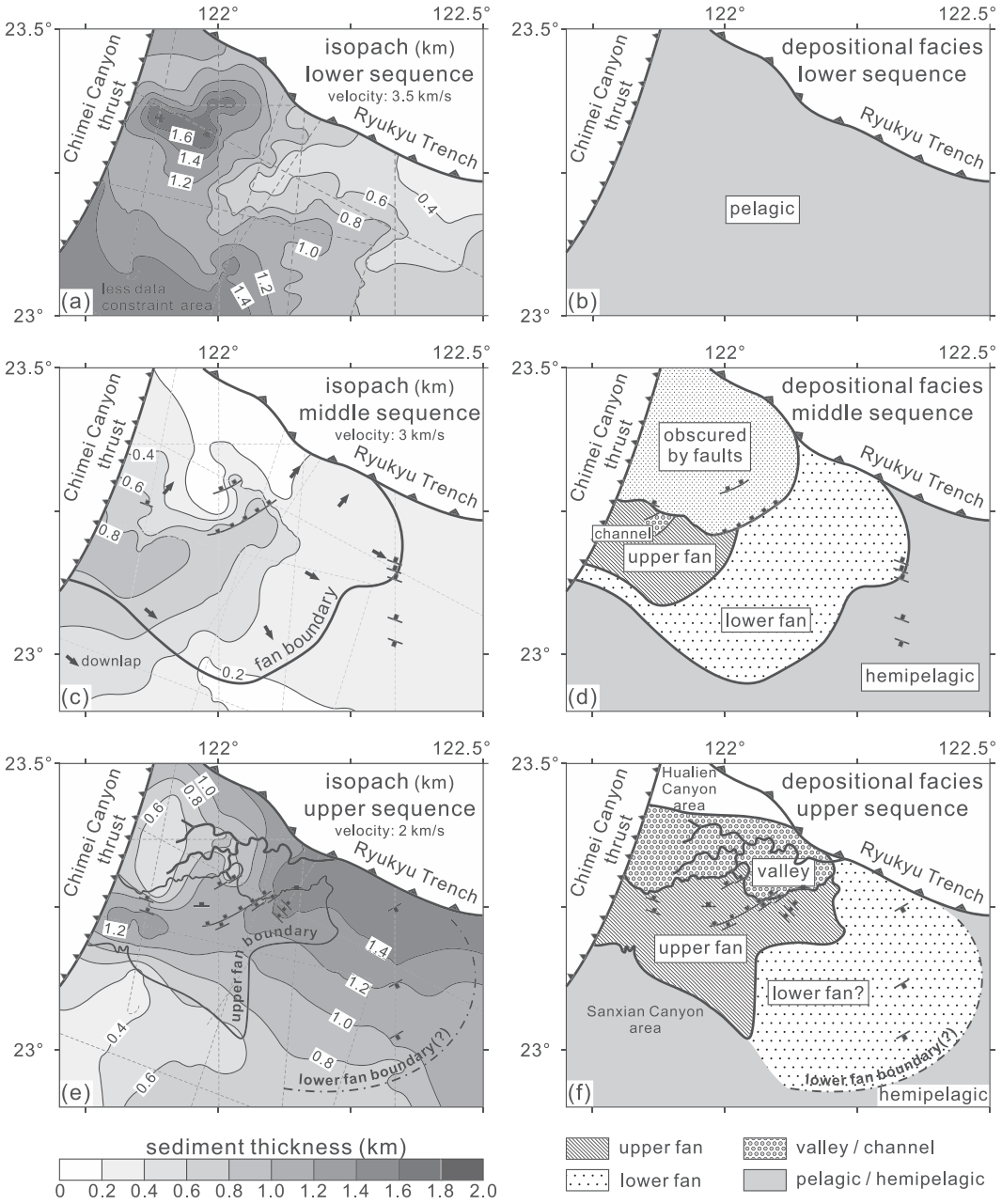

Figure 12. (a, c, and e) Isopach and (b, d, and f) distribution of seismic facies assemblage of the three seismic sequences east of the Chimei Canyon thrust. The thickness of seismic sequence is calculated based on the average velocity of each seismic sequence, which is obtained by the velocity analysis of seismic CMP gathers (applied velocity is shown in each figure).

The thickness of the lower seismic sequence is 0.6–1.8 km (Figure 12). This thickness variation represents infilling over the original relief of the Huatung Basin oceanic crust, as can be seen by inspection of seismic profiles (Figures 8, 10, 11, and S1–S5). In particular, the lower part of lower sequence shows large thickness variations over basement relief, whereas the upper part of the lower sequence shows relatively constant thickness (e.g., Figures 8 and S1). Based on seismic facies, amplitude, and thickness distribution, we interpret that the lower seismic sequence is pre-collisional sequence of sediments deposited before the arc-continent collision, with its development of orogenic source-to-sink pathways. Figure 12b shows the distribution of depositional facies.

5.3.2. Seismic Facies of the Middle Seismic Sequence

The transparent wedge-shaped seismic facies (seismic facies 2) is dominant in the middle seismic sequence. The yellow color in Figures 10 and 11 shows examples of this seismic facies. The reflections of this seismic facies show downlap on the lower seismic sequence along sequence boundary *Y*. However, because the amplitudes within this seismic facies are very weak, it is not easy to identify the downlap pattern. In highly distal areas, they may represent a transition to a transparent hemipelagic variety of seismic facies 1 (e.g., Figures 8, S1, and S6). In seismic sections perpendicular to the mountain belt, the external shape of this seismic facies is wedge shaped, which thickens toward mountain belt (source area) but thins toward the center of the Huatung Basin (Figures 14 and S6). In the seismic sections parallel to the mountain belt, the external shape appears mound shaped (Figures 8, 10, and S1–S3). We interpret this seismic facies in the middle sequence as the distal overbank deposits of the Chimei Fan.

The Chimei Fan in the middle sequence covers an area of 2,087 km^2, with maximum thickness of ~0.8 km (Figure 12c). The isopach map shows that the middle seismic sequence thickens westward toward Taiwan mountain belt, and thins eastward toward the center of the Huatung Basin (Figure 12c). The upper fan seismic facies assemblage is distributed closer to Taiwan mountain belt and the lower fan seismic facies assemblage is distributed around the upper fan (Figure 12d). The transparent pelagic seismic facies is distributed far away from the mountain belt and may be hemipelagic (Figure S1). Based on the seismic facies distribution and thickness, we consider that the Chimei Fan in the middle sequence reflects the onset of source-to-sink transport pathways from the Taiwan arc-continent collision, which are not seen in the lower seismic sequence. This transition is marked by the abrupt onset of transparent distal seismic facies across seismic sequence boundary *Y*.

5.3.3. Seismic Facies of the Upper Seismic Sequence

Seismic facies in the upper seismic sequence are generated in high-energy environments. The seismic facies in the upper fan includes high-continuous divergent configuration seismic facies (seismic facies 3), hummocky, high-amplitude onlapping-fill seismic facies (seismic facies 5) and chaotic seismic facies (seismic facies 6). The seismic facies within the lower fan includes facies 3 and 6 but lacks facies 5. The blue, green, and orange colors in Figures 10 and 11 show examples of those seismic facies.

In the upper fan, the low-amplitude, high-continuous divergent configuration seismic facies (facies 3) is present as levee. The levee south of the deep-sea valley may be old and inactive. Hummocky, high-amplitude onlapping-fill seismic facies (facies 5) is present in the deep-sea valley near the foot of the Chimei Canyon (Figures 10a and 10b). We interpret the seismic facies 5 as channel-fill deposited at the foot of the Chimei Canyon (Figure 10a). A dendritic deep-sea channel system (Figures 3, 10c, 10d, 11a, and 11b) formed and may transport sediment from Chimei Canyon to the Hualien Canyon at longitude 122.16°E (Figures 3, 11c, and 11d), and finally the Hualien Canyon merges into the Ryukyu Trench.

The thickness and distribution of the upper seismic facies are shown in Figures 12e and 12f. The isopach map shows that the maximum thickness of the upper seismic sequence is 1.4 km near the Ryukyu Trench and 1.3 km in the Chimei Fan and that the thickness increases toward the upper fan near the Taiwan mountain belt and decreases toward the center of the Huatung Basin. The thickening of the upper sequence toward the Ryukyu Trench reflects that the basin is primarily developing accommodation toward the north due to flexure into the subduction zone. Therefore, we could not see the obvious thickening of the Chimei Fan westward to the Taiwan mountain belt based on isopach map of the upper sequence.

Comparing the middle seismic sequence of the Chimei Fan with the upper sequence shows that the upper sequence has noticeably larger levees and channels. The upper sequence of the fan may therefore reflect a larger volume of sediment dumped into the Huatung Basin as the depocenter shifted from the forearc basin to the Huatung Basin after 1 Ma. As the Luzon Arc and forearc basin were deformed and uplifted, terminating the forearc basin depocenter ~1 Ma, the orogenic sediment bypassed the forearc basin and started to be deposited entirely in the Huatung Basin, forming the Chimei Fan in the upper sequence.

The western Chimei Fan within the Offshore East Taiwan thrust belt represents a wedge-top depocenter with progressive structural uplift and associated incision (~1 km), forming the present Chimei Canyon (Figure 7b). This uplifted and deformed fan is preserved in the Changping High and Takangkou High (Figure 4; section 6.3). Comparable incision is also present in the eastern Chimei Fan where structural uplift is missing; therefore, highly erosive flows appear likely to have produced the present morphology

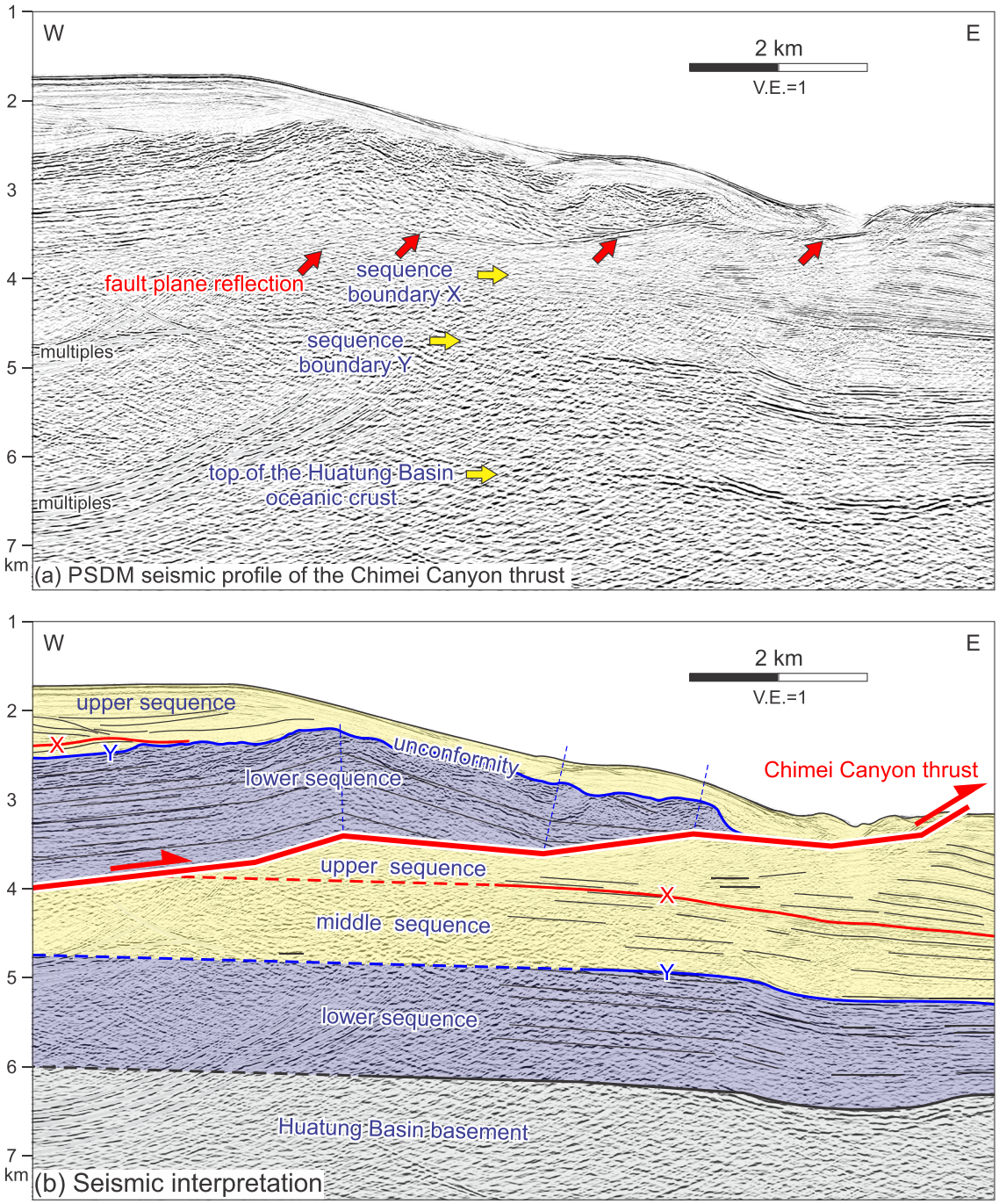

Figure 13. Detail of prestack depth migrated short-streamer seismic profile MCS914-11 (Figure 14), along the southern Chimei Canyon wall, imaging the Chimei Canyon thrust. The map location is shown in Figure 4.

of the Chimei Canyon-Fan system. The preferential destruction of the northern part of the eastern Chimei Fan by submarine erosion relative to the largely preserved southern part of the eastern Chimei Fan potentially reflects the same progressive northward plate flexure of the Huatung Basin lithosphere associated with Ryukyu Trench subduction, as discussed previously for the Chimei Canyon (section 4.1). Furthermore, the southern part of the eastern Chimei Fan has been subject to northward gravity sliding and formed of slump scarps along the northern rim of the remnant part of the Chimei Fan (Figures 3d, 10, and 11).

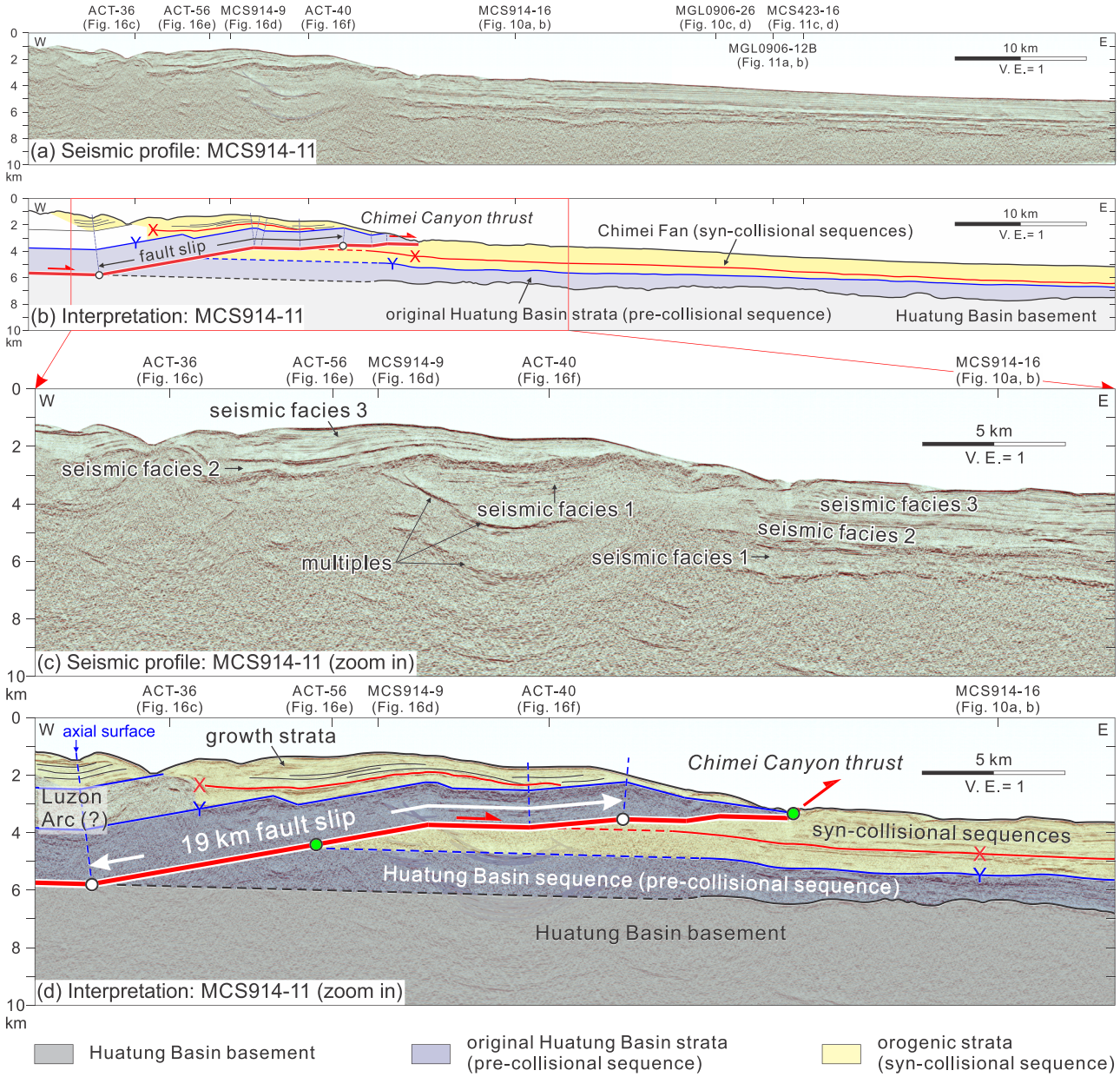

Figure 14. (a) Prestack depth migrated short-streamer seismic profile MCS914-11 along the southern Chimei Canyon wall and Chimei Fan. This seismic profile shows that the Chimei Fan has been uplifted by the Chimei Canyon thrust. A detail of the section at the toe of the thrust is shown in Figure 13. (b) Seismic interpretation. (c) Zoom in part of the seismic profile (a) and its interpretation (d). See Figure S6 for higher-resolution images.

6. Structures

The Chimei Canyon-Fan system has been deformed by a series of east-vergent thrusts (Lin, 2010). The thrusting is much more highly imbricated along the canyon axis, where there is >1-km incision, than along the south flank where the fan is largely intact, as described in the following sections (Figures 13, 14, 15, S6, and S7).

6.1. Seismic Profile South of the Chimei Canyon

The EW seismic profile MCS914-11 (Figures 13 and 14) runs 5–10 km south of the Chimei Canyon (Figures 4 and 6). This is a short-streamer (~1 km) legacy line that we have reprocessed using prestack depth migration, which sufficiently improved the image for interpretation in depth, especially near the toe of the thrust

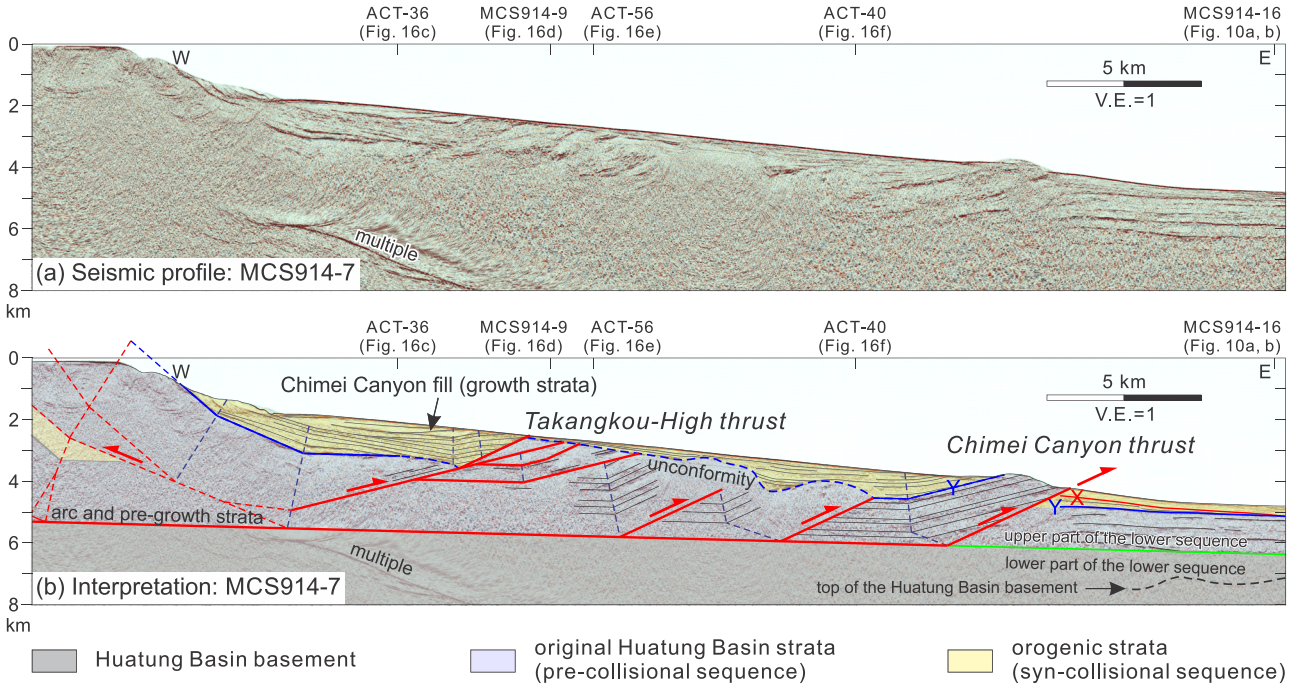

Figure 15. (a) Prestack depth migrated short-streamer seismic profile MCS914-7 along the Chimei Canyon. The profile shows tilted pregrowth strata (lower seismic sequence, purple) and slightly deformed growth strata (middle and upper seismic sequence, yellow). The frontal thrust is best imaged in this profile and defines the lower limit of the Chimei Canyon. (b) Seismic interpretation. The red solid lines are the thrusts and detachment. Red dashed lines are less certain thrusts. The west-vergent structures at the west end of the profile, which are thought to be responsible for the steep headwall of Chimei Canyon, are interpreted from surface geological data onshore Coastal Range (see Figure 17). See Figure S7 for higher resolution images.

(Figure 13 detail). This imaging shows a shallow anticline and fault ramp structure in the hanging wall, with fault plane reflectors, and undeformed Huatung Basin strata in the footwall down to the top of oceanic crust (Figure 13).

Six observations are crucial to seismic interpretation: (1) Strata on the east flank of the anticline dip into the fault and display hanging wall cut-offs (Figure 13), whereas strata on the west flank appear parallel to the fault for a distance of about 19 km to the west (Figure 14). These are typical features of classic ramp-flat fault-bend fold anticlines and lead directly to the present structural solution (Mount et al., 1990; Shaw et al., 2004; Suppe, 1983). (2) The three seismic sequences in the Huatung Basin can be traced in the footwall for about 5 km to the west of the surface trace of the Chimei Canyon thrust, with horizontal reflectors becoming progressively fainter (Figure 13). (3) The stratigraphic correlation between the hanging wall and footwall is regionally unambiguous, as discussed more fully below, with both showing seismic facies 1 in the basal unit, characteristic of the pre-collisional pelagic Huatung Basin sequence, with thicknesses that are regionally typical (Figures 13 and 14c). Overlying strata show facies 2 and 3 in the hanging wall and footwall consistent with sequences 2 and 3 but are thinner and more variable in thickness and geometry in the hanging wall, consistent with their being growth strata (Figure 14). There is an erosional unconformity at the top of the lower sequence that is confined to the top of the hanging wall anticline at the toe of the Chimei Canyon thrust, which indicates that the toe of the thrust was exposed to submarine erosion at the initial stage of thrusting. (4) The hanging wall thickness of the Huatung Basin lower sequence west of the anticline is consistent with a bedding-parallel detachment along the top of oceanic crust, which has been confirmed by restoration. There is no indication of basement involvement in this structure. In particular, the strong top of basement reflection observed widely in the autochthonous Huatung Basin (Figure 14a) is missing everywhere in the hanging wall at depths at which it would otherwise be expected to be imaged (Figures 13 and 14c). (5) Two narrow east-facing monoclinal flexures are present in the lower sequence in the hanging wall (middle and top of the main thrust ramp). Associated thickness changes in overlying strata indicate growth during the upper part of the middle sequence and lower part of the upper sequence. These flexures are interpreted to mark changes in thickness of the lower sequence across faults in the oceanic crust, producing an overall westward thickening of the Chimei Canyon thrust sheet. Similar

magnitudes of abrupt thickness change across basement relief are widespread in the undeformed Huatung basin (e.g., Figures S1 and S6). (6) The ramp-flat interpretation for the active Chimei Canyon frontal thrust, which is stepping up from a regional detachment above the top of Huatung Basin crust, requires that there is an active synclinal axial surface extending from the base of the ramp to the seafloor that is tied to the base of the ramp where the Chimei Canyon thrust flattens to the detachment above the top of Huatung Basin crust. This axial surface is observed ~2 km east of the west end of the seismic line. The associated footwall cut-off corresponds to the hanging wall cut-off under the shallow hanging wall anticline, defining a total displacement of ~19 km on the Chimei Canyon thrust (Figure 14d).

In the footwall of the Chimei Canyon thrust, the seismic reflection profile reveals sedimentary layers and the top of the Huatung Basin basement. These autochthonous sedimentary layers extend westward beneath the Chimei Canyon thrust (Figure 13). The three seismic sequences in the Huatung Basin described in the previous section are well defined in the footwall on this seismic reflection profile. Based on seismic facies analysis, we correlate seismic sequences of between the hanging wall and footwall (Figure 14). The lower seismic sequence of the footwall (the Huatung Basin lower sequence) is correlated to the lower seismic sequence of the hanging wall. The transparent middle and upper seismic sequences in the footwall are correlated to the middle and upper seismic sequences in the hanging wall. Therefore, the frontal thrust has 19-km horizontal slip and 2.6-km maximum uplift (Figure 14), with associated uplift and incision of the western Chimei Fan. The seismic profile MCS914-9 (Figure 16d), which is a strike line, shows thick strata in the southern and northern canyon walls (the Changping High and Takangkou High), which we interpret as the uplifted proximal Chimei Fan. The beginning of thrusting is the uppermost middle sequence just below sequence boundary *X*, as shown by growth strata over the abrupt monoclinal flexures and erosional growth unconformity in the frontal anticline (Figures 14 and S6).

6.2. Seismic Profile Along the Canyon Axis

Chimei Canyon runs across a series of east-vergent thrust faults offshore eastern Taiwan (Figure 15); nevertheless, the canyon floor is generally very smooth without obvious fault scarps except where the canyon crosses the Chimei Canyon thrust at the foot of the canyon (Figures 3, 4, and 7). A short streamer (~1 km) legacy seismic reflection depth profile along the Chimei Canyon axis (MCS914-7) shows that strata interpreted to be largely lower seismic sequence have been deformed and thrust eastward in a series of about five incompletely imaged thrust imbrications (Figure 15 purple strata). Thus, this axial canyon section is substantially more complex structurally than the adjacent section to the south of the canyon which shows a single, relatively long and intact thrust sheet (Figures 13 and 14).

The observed along-strike change from a single intact thrust sheet south of the canyon to a series of thrust imbrications along the canyon axis is not surprising from the perspective of critical-taper wedge mechanics because canyon erosion reduces the thickness and hence the strength of the Chimei Canyon thrust sheet causing it to deform until it reaches critical taper (e.g., Dahlen & Suppe, 1988; Davis et al., 1983; Fuller et al., 2006; Liu et al., 2020; Suppe, 2007). The canyon section has a taper of ~4°, which must be approximately critical because it is actively deforming both internally and at the toe (Figure 15). In contrast, syntectonic submarine-fan sedimentation, which tapers in the direction of thrust motion, has strengthened the thrust sheet south of Chimei Canyon, giving it a strongly tapered geometry (Figure 14), allowing it to remain intact in spite of its complex ramp-flat geometry and folding of the overlying fan surface. Chimei Fan deposition (seismic facies 2 and 3) over the thrust sheet has increased its taper to ~8° from its ~2° taper in the basal pregrowth strata (Figure 14), which is twice the ~4° critical taper along the canyon axis (Figure 15). Therefore, active fan and canyon surface processes have made an observable impact on the mechanics of the underlying Chimei Canyon thrust system.

The stratigraphic assignment within the imbricate thrust structure is less certain because of image quality, but displays seismic facies 1 in the hanging wall and footwall of the Chimei Canyon frontal thrust and is therefore assigned to the basal Huatung Basin sequence. The location of top of basement is constrained by the crossing line MCS914-16 (Figure 10a) just east of the frontal thrust, which ties to the adjacent dip section south of the canyon (Figures 13 and 14). The regional dip within the thrust belt is assumed to be the same as the undeformed foreland to the east, similar to Figure 14. The depth of the basal detachment is constrained by the geometry of folding above the frontal thrust (Figures 15 and S7). This stratigraphic level appears to be significantly above the top of the Huatung Basin oceanic crust based on correlation from the frontal thrust to the crossline MCS914-16 (Figure 10a), which is close to the boundary between the upper lower sequence and the lower sequence.

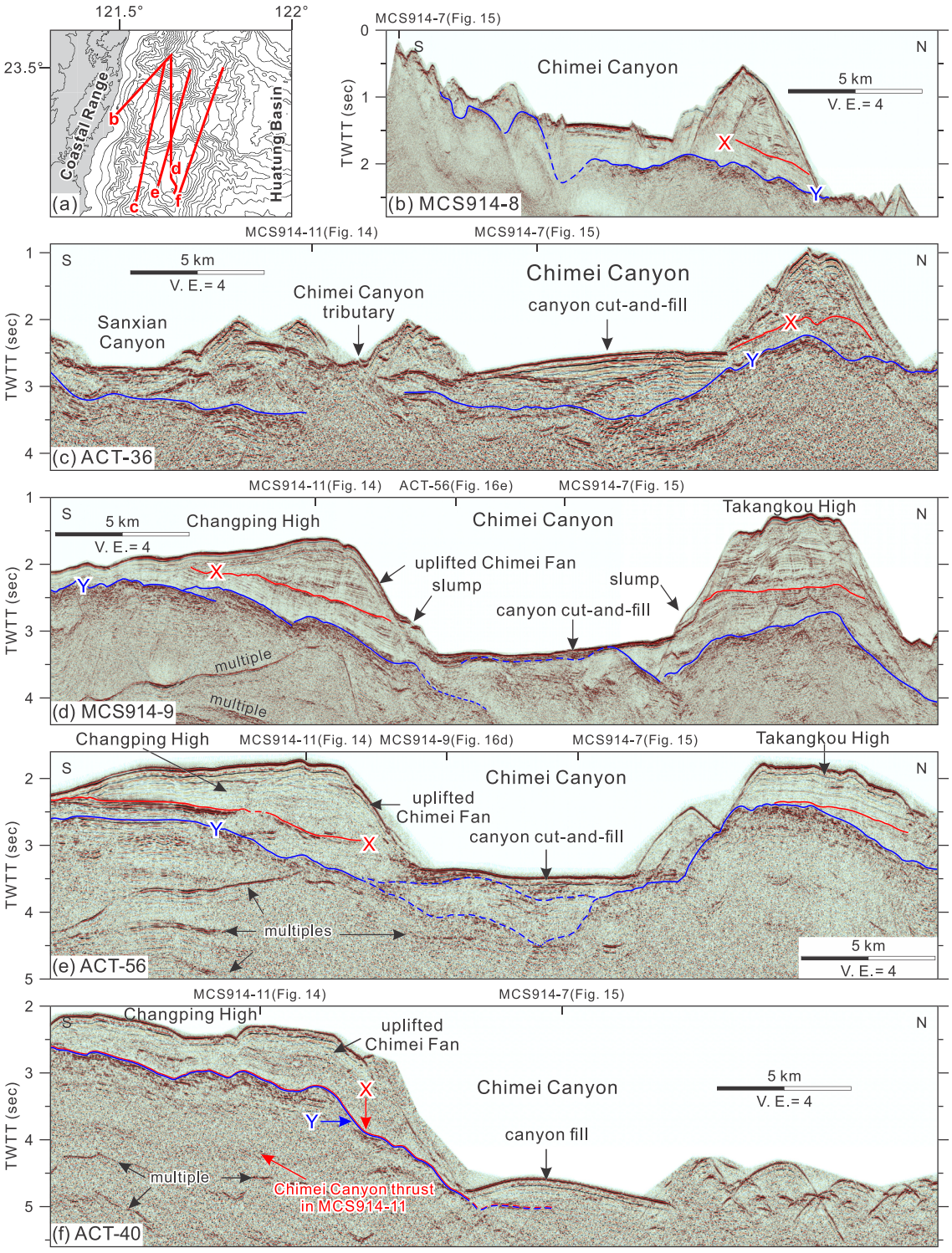

Figure 16. Seismic profiles across the Chimei Canyon from upstream to downstream. Location of each seismic profile is show in (a). Two seismic sequence boundaries *X* and *Y* are shown.

The deformed strata near the seafloor have been truncated by erosion, and thin young canyon-fill sediment covers the older deformed strata, making the active canyon floor a smooth, planar east-dipping surface (Figures 3, 4, 15, and S7). The two most recently active thrusts (the Takangkou High thrust and the Chimei Canyon thrust) cut through to the seafloor (Figure 15) and caused seafloor deformation (Figures 3

and 4). The orientation of Chimei Canyon in the vicinity of the Takangkou High thrust changes from NW-SE trending west of the fault zone to E-W trending east of the fault zone. Near the west end of the seismic profile (Figure 15), the strata are tilted eastward, producing a broad syncline, which marks the transition to the west-vergent thrust imbrications of the largely onshore Coastal Range thrust belt (discussed in section 6.4).

The imbricate thrusts display several structural styles. Hanging wall strata of the frontal Chimei Canyon thrust dip west 14°, which is less than the 25° dip of the fault plane, and flatten down dip to horizontal, constraining a depth to the detachment close to the top of Huatung Basin crust. The back synclinal axial surface extends to the seafloor indicating that it is geomorphically active, with growth strata showing a fanning of dips. This geometry is classic shear fault-bend folding geometry (Le Béon et al., 2019; Shaw et al., 2004; Suppe et al., 2004; Yue et al., 2005, 2011). The next two thrust imbrications to the west are less well imaged but sufficiently imaged to identify synclinal axial surfaces that constrain the location of thrust ramps. The Takangkou High thrust shows shallow imbrications in the footwall and shallow folded growth strata in the hanging wall. At the west end of MCS914-7 profile (Figure 15), there is a major syncline that marks the bathymetric headwall of Chimei Canyon and the transition to the west-vergent Coastal Range thrust belt, which is characterized by steeper faults and higher uplift.

6.3. Seismic Profiles Across the Chimei Canyon and Distal Chimei Fan

Figure 16 presents a series of NS seismic profiles that run across the Chimei Canyon from proximal to distal, showing the smooth canyon bottom and steep canyon walls. Submarine fan deposits are imaged in the adjacent Changping High and Takangkou High, which are up to ~1,500 m thick and truncated by the canyon walls, consistent with deep incision (Figure 16). Only limited strata are deposited in the canyon bottom. Based on the seismic facies analysis, the facies on both sides of the canyon walls can be correlated to three seismic sequences, separated by seismic sequence boundaries *X* and *Y*. These time-migrated strike lines with large sea-bottom relief are insufficiently imaged at the depths required to constrain the transition between the imbricated thrust structures of the Chimei Canyon section (MCS914-7, Figure 15) and the long intact thrust sheet of the Changping High section to the south (MCS914-11, Figure 14).

Seismic profiles across the distal Chimei Fan, east of the frontal thrust, show inward dipping normal faults along the flanks of the deep-sea valley, dropping strata down into the valley (Figures 10, 11, and S2–S5). These represent near surface collapse of valley and canyon walls because they do not penetrate seismic horizon *Y* into the lowest seismic sequence but rather detach in the distal strata of the middle sequence or above. This interpretation is consistent with the arcuate shapes of the fault scarps in plain view (Figures 3c and 3d). Inward dipping normal faults may also exist along the flanks of the Chimei Canyon (Figure 16).

6.4. Relationship Between Offshore and Onshore Thrust Belts

Here, we present the relationship between the Offshore East Taiwan thrust belt and the Coastal Range thrust belt as shown in a combined onshore-offshore cross section (Figure 17) along the current wedgetop Chimei Canyon-Hsiukuluan River transport pathway (Figure 4). The offshore section is along the axis of the upper Chimei Canyon which is approximately in the plate convergence direction and consists of the interpreted seismic section of Figure 16, projected into the convergence direction (Figures 4 and 6). The onshore portion utilizes the cross section of Chi et al. (1981), augmented by data from Wang and Chen (1993) and Shyu et al. (2006).

The structure of the Coastal Range thrust belt is dominated by west-vergent thrust faults that in map view run parallel to the map traces of hanging wall stratigraphy, with very large strike length to thickness ratios (Figure 4). This map pattern is characteristic of thin-skinned imbricated thrust-belt structure (e.g., Suppe, 1985; Yue et al., 2005, 2011). The detachment horizon of the Longitudinal Valley thrust along the cross section is in early Pleistocene forearc basin strata but the more interior Chimei, Huatungshan, and Takangkou thrusts run along detachments at the base of the Miocene Tuluanshan arc volcanics (Figure 4 and map of Wang & Chen, 1993). Therefore, the Coastal Range thrust belt is detached from the Luzon Arc and forearc lithosphere at a shallow depth, indicated by the stratigraphic thickness of the thrust sheets (~5 km or less, Figure 17). The original footwall of these Coastal Range thrust sheets, which was arc and forearc lithosphere, has been subducted as proposed by Chemenda (Boutelier et al., 2003; Chemenda et al., 1997; Chemenda, Hurpin, et al., 2001; Chemenda, Yang, et al., 2001) and imaged in regional tomography (e.g., Huang et al., 2014).

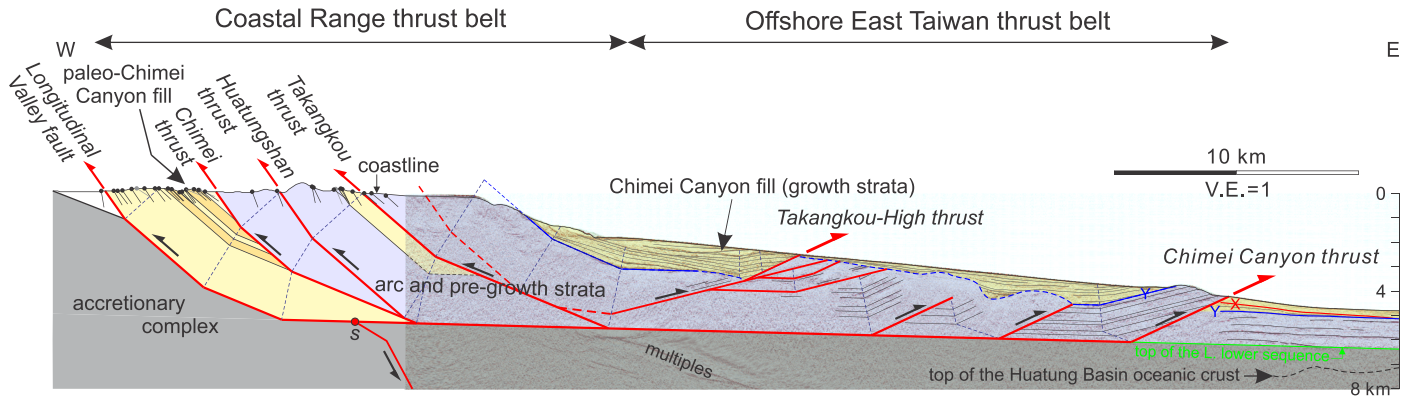

Figure 17. Combined onshore-offshore structural section along the wedge-top Hsiukuluan River-Chimei Canyon transport pathway (Figure 4). The shortening is ≳60 km, which is largely post 1 Ma and is consistent with present-day ~60 mm/yr geodetic shortening rate. The eastern limit of Chimei Canyon is morphologically defined by the Chimei Canyon frontal thrust and the western limit by the rapidly uplifting (5–20 mm/yr) west-vergent Coast Range thrust belt that produces the steep headwall of Chimei Canyon (Figure 4). Shortening of the combined onshore and offshore thrust belts is linked at deeper crustal levels to the secondary subduction of arc and forearc lithosphere and accretionary complex at an "S point," as proposed by Chemenda (Boutelier et al., 2003, Chemenda et al., 1997; Chemenda, Yang, et al., 2001; Huang et al., 2014). Structural interpretation of onshore Coastal Range Hsiukuluan River cross section is modified from Chi et al. (1981) and the offshore Chimei Canyon section is a projection of Figure 15 into the plate convergence direction.

In contrast with the Coastal Range thrust belt, the active Offshore East Taiwan thrust belt underlying the wedge-top Chimei Canyon and fan is characterized by east-vergent thin-skinned thrusting above a detachment within or at the base of the pre-orogenic Huatung Basin seismic sequence (lower sequence), above the top of oceanic basement (Figures 14 and 15). This detachment level must extent at least 20 km to the west given the ~20 km observed offshore shortening. Therefore, this detachment must extend under the west-vergent Coastal Range thrust belt as shown in the combined onshore-offshore cross section in Figure 17. However, the original footwall of the Coastal Range thrusts is shallower stratigraphically than the Lower Cretaceous base of the Huatung Basin pelagic sequence, which possibly extended to the west below the Miocene Luzon Arc volcanics prior to thrusting as suggested by the Lower Cretaceous radiolarian cherts found on Lanyu Island (section 7.1.1). The total shortening of the combined onshore-offshore thrust belt (Figure 17) is >62 km, which at the present geodetic shortening rate of ~60 mm/yr is consistent with ~1 Ma of deformation for the observed structures.

7. Discussion

7.1. Evolution of the Chimei Canyon-Fan System

We propose a simple model for the development of the Chimei Canyon-Fan system and how it records the onset and progression of the Taiwan arc-continent collision. In section 5, we documented three seismic sequences in the Huatung Basin (Figure 8): (1) The lower seismic sequence is dominated by widespread sheet-drape seismic facies, which indicates pelagic-dominated sediments without direct collision-related sources. (2) The middle seismic sequence records the first transport of sediments from the Taiwan mountain belt across the Luzon Arc and into the deep Huatung Basin, forming the initial distal Chimei Fan (Figures 12c and 12d). According to our preferred model, this accumulated between ~2 and 1 Ma when the Taiwan mountain belt started to undergo accelerated uplift, exhumation, and erosion (Byrne et al., 2011; Hsu et al., 2016), and when the marine forearc basin, now exposed onshore in the Coastal Range, records a very rapid increase in sedimentation that terminated ~1 Ma (Figure 5). (3) The upper seismic sequence is interpreted to have been deposited after ~1 Ma when the depocenter shifted entirely to the deep Huatung Basin east of the arc, associated with ~60-km shortening of the Coastal Range and Offshore Eastern Taiwan thrust belts in the last ~1 Ma (Figure 17). A deforming wedge-top setting for the Chimei Canyon and Fan is indicated by growth strata beginning in the uppermost middle sequence and continuing through the upper sequence (section 6.1).

The age assignments of these events in the Huatung Basin and their correlation with events onshore are necessarily tentative because there are currently no direct observational constraints on the ages of the

Table 2
Two Age Models for the Chimei Fan and Huatung Basin Sequences, With Estimated Sedimentation Rates

(a) Two age models for the Chimei Fan sequences with estimates of sedimentation rate		
	Preferred model	Alternative model
Age of base of upper sequence (seismic sequence boundary *X*)	1 Ma	2 Ma
Age of base of lower sequence (seismic sequence boundary *Y*)	2 Ma	4 Ma
Thickness upper sequence	1,050–1,400 m (1,200 m average)	
Thickness middle sequence	290–800 m (470 m average)	
Sedimentation rate: seismic facies 3–6 (upper sequence)	1,050–1,400 m/my 1,200 m/my (average) Agrees with Table 3, piston core, and deformation rate	525–700 m/my 600 m/my (average) Disagrees with Table 3 and deformation rate
Sedimentation rate: seismic facies 2 (middle sequence)	290–800 m/my 470 m/my (average) Reasonable relative to 1–2 Ma forearc rate (Figure 5)	145–400 m/my 235 m/my (average) Likely too fast relative to 2–4 Ma forearc rate (Figure 5)
(b) Two age models for the lower Huatung Basin sequence with estimates of sedimentation rate		
	Preferred model	Alternative model
Age of upper part of lower sequence, with presumed Luzon Arc input	2–15 Ma	4–15 Ma
Age of lower part of lower sequence	15–130 Ma	15–35 Ma
Thickness upper part of lower sequence	371–920 m (665 m average)	
Thickness lower part of lower sequence	70–760 m (508 m average)	
Sedimentation rate: seismic facies 1 and 6 (upper part of lower sequence)	29–71 m/my 51 m/my (average) Reasonable for hemipelagic with arc input	34–84 m/my 60 m/my (average) Reasonable for hemipelagic with arc input
Sedimentation rate: seismic facies 1 (lower part of lower sequence)	0.6–6.6 m/my 4.4 m/my (average) Typical deep-ocean pelagic sedimentation rate	3.5–38 m/my 25 m/my (average) Too fast deep-ocean pelagic rate without other input

offshore seismic sequence boundaries of the Chimei Canyon-Fan (the middle and upper seismic sequences) or of the underlying lower Huatung Basin seismic sequence. Nevertheless, we can apply indirect constraints to infer their ages. These constraints include: (1) stratigraphic constraints from the Plio-Pleistocene forearc basin, now exposed on-land in the Coastal Range (Figure 5; Table 2); (2) estimates of the ages of the three seismic sequences based on their seismic facies and thickness distributions and probable rates of deposition (Table 2); (3) estimates of the erosive flux of sediment from the Hsiukuluan River drainage combined with estimates of the total preserved volume of sediment in the upper seismic sequence of the Chimei Fan and the frontal part of the Ryukyu accretionary wedge (Table 3). Two plausible age models are summarized in Table 2 with their implications for sedimentation rate.

7.1.1. Lower Seismic Sequence: Before Chimei Canyon-Fan System Development

The lower seismic sequence is dominated by basinal widespread sheet-drape seismic facies. The *P* wave velocity of the lower sequence is 3.5–4.5 km/s, which is measured by our seismic reflection PSDM velocity analysis and by OBS data (Klingelhoefer et al., 2012). Based on seismic facies, amplitude, *P* wave velocity, and thickness (section 5.3), we suggest that the lower seismic sequence consists of pelagic sediment that accumulated in a distal oceanic setting before the onset of input of orogenic detritus from the Taiwan arc-continent collision.

The age of the Huatung Basin oceanic crust is still controversial with diverse proposals. Cenozoic interpretations include Miocene to Oligocene (15–30 Ma) based on Rayleigh-wave phase velocities similar to the South China Sea (Kuo et al., 2009) and middle Eocene to late Eocene (36–41 Ma, Hilde & Lee, 1984; ~51 Ma, Sibuet et al., 2002; 41–33 Ma, Doo et al., 2015), similar to the West Philippine Basin, based on interpretation of marine magnetic anomalies. Early Cretaceous (~119–131 Ma) is proposed based on modeling of marine magnetic anomalies in the central and northern Huatung Basin, seismic velocity modeling (Eakin et al., 2015) and Ar/Ar cooling ages of dredged gabbros at two locations in the southern Huatung Basin (Deschamps

Table 3
Estimated Source-to-Sink Mass-Balance Constraint on Age of Chimei Fan Upper Sequence

Source			
Present-day source	Present source area	Denudation rate	Eroded rock volume/my
Hsiukuluan River drainage	1,891 km^2	4–5 km/my	7,564–9,455 km^3/my
Sum of source as eroded rock volume	7,564–9,455 km^3/my		
Sink			
Preserved sinks	Cross-sectional area	Strike length	Preserved volume
Chimei submarine canyon (canyon wall strata)	22 km^2	19 km	418 km^3
Chimei Fan	83 km^2	49 km	4,067 km^3
Chimei Fan (below thrust)	14 km^2	35 km	490 km^3
Ryukyu accretionary wedge close to the Chimei Fan	85 km^2	47 km	3,995 km^3
Sum of sinks as sediment volume	8,970 km^3		
Sum of sinks as eroded rock volume[a]	7,176–8,073 km^3		

Note: The preserved sink volume in the upper seismic sequence is approximately equal to 1 Ma of eroded volume at the present erosion rate and source area (largely Hsiukuluan River drainage area, Figure 3), in agreement with an age of ~1 Ma for the base of the upper seismic sequence (see section 7.1.3).
[a]Computed using a ratio of sediment density to rock density of 0.8 to 0.9.

et al., 2000; Deschamps & Lallemand, 2002; Lallemand, 2016). Yeh and Cheng (2001) found Early Barremian (~115 Ma) radiolarian chert fragments in volcanic breccias of the Luzon Arc on Lanyu Island (Figure 2) and suggested that these fragments were brought to the surface in volcanic eruptions from Early Cretaceous oceanic crust underlying the Luzon Arc in this region. The radiolarian fauna is similar to low-latitude faunas found in ocean drilling in the central North Pacific. Dimalanta et al. (2020) suggest that the Huatung Basin may be a remnant of Mesozoic proto-Philippine Sea Plate based on geochemical correlation of allochthonous crust-mantle sequences along the eastern edge of the Philippines.

The basin widespread sheet-drape seismic facies (seismic facies 1) that dominates the lower seismic sequence in the Huatung Basin (Figures 9 and S1) shows deep ocean pelagic sediment characteristics. The similar seismic facies are imaged in the northwestern Pacific at deep basin ODP sites 800, 801, and 1,149 (5,600–5,800 m), where they correspond to Cretaceous and Jurassic interbedded radiolarite, radiolarian chert, porcellanite, and siliceous clay on the top of oceanic crust, with overlying Cenozoic abyssal red clay (Lancelot et al., 1990; Plank et al., 2000). Sites 800 and 801 contain the addition of middle Cretaceous volcaniclastic deposits associated with midplate volcanism of the Magellan Seamount Province. Similar seismic facies are imaged in Cenozoic pelagic sediments the West Philippine Basin (Higuchi et al., 2007; Ingle et al., 1975).

The lower part of the lower Huatung Basin seismic sequence is wholly sheet-drape seismic facies (seismic facies 1) whereas the upper part contains the addition of interbedded chaotic seismic facies (seismic facies 6, Figure S1), which is interpreted as mass transport deposits (Sangree & Widmier, 1977). The chaotic seismic facies becomes more widespread toward the Luzon Arc, so it may represent distal input from the Luzon Arc after it was established ~15 Ma. Furthermore, the pelagic sheet-drape seismic facies in the upper part of the lower sequence would be expected to contain fine grained volcanic input from the Luzon Arc, which may contribute to the higher seismic amplitudes relative to the more transparent lower part of the lower sequence (Figure S1).

Here, we use sediment thickness to estimate the compacted sedimentation rate for the lower seismic sequence, based on two end-member models of the age of magnetic anomalies of the northern Huatung Basin oceanic crust in the area of the Chimei Fan: (1) Early Cretaceous (130 Ma) from Deschamps et al. (2000) and (2) mid-Cenozoic (30 Ma) from Doo et al. (2015) based on the most complete magnetic anomaly data set (Table 2, b). We fix the boundary between the upper and lower parts of the lower sequence (Figure S1) at 15 Ma, which is the approximate age of the beginning of the Luzon Arc. The thickness of the lower sequence is 600–1,800 m, with the upper lower sequence at a relatively constant 600 m and the lower sequence contribution most of the variation reflecting the relief of the top of oceanic crust (average 500 m). The Early Cretaceous (130 Ma) and mid-Cenozoic (30 Ma) crustal ages yield two sets of model sedimentation rates

given in Table 2, b, which we now compare with known sedimentation rates for ocean drilling sites with similar seismic facies to the Huatung Basin.

The lower part of the lower Huatung Basin sequence yields an average sedimentation rate of 4.4 m/my for the 130-Ma Early Cretaceous model, which is a very typical oceanic pelagic sedimentation rate below the carbonate compensation depth as outlined as follows. In contrast the 25 m/my, rate for the 30-Ma mid-Cenozoic model would require special explanation such as input volcanic material. DSDP site 291 east of the Philippine Trench (5,217-m water depth) gives an Eocene to present rate of 4.1–4.2 m/my for nannofossil and radiolarian pelagic clays (120 m) (Ingle et al., 1975). DSDP site 292 east of Luzon on Benham Rise oceanic plateau (2,943-m water depth) gives a late Eocene to present rate of 8.5–12 m/my for pelagic chalk and nannofossil ooze deposited above the carbonate compensation depth, which is much shallower than the >5,000-m depth of the Huatung Basin (Ingle et al., 1975). Pelagic sediments in the deep-water West Philippine Basin widely have a thickness of <200 m away from bathymetric highs and troughs, implying average rates of <5–7 m/my (Higuchi et al., 2007). In the western Pacific IODP site 1149 east of the Izu-Bonin trench (5,829-m water depth) drilled into sheet-drape seismic facies gave a rate of 20 m/my for lower Cretaceous radiolarian chert and siliceous nannofossil marls deposited above the carbonate compensation depth with overlying radiolarian cherts and brown pelagic clays giving an average rate of 1.4 m/my (Plank et al., 2000). ODP sites 800 and 801 east of the Mariana trench (5,685-m water depth) show sheet-drape seismic facies (Lancelot et al., 1990). Sedimentation rates at site 800 are 2–6 m/my in pelagic clays and radiolarian chert, which increase to 12–35 m/my in the mid-Cretaceous interval with volcaniclastic input from the Magellan Seamount Province. Sedimentation rates at site 801 are 1–10 m/my in radiolarite and brown chert and porcellanite intervals in the Jurassic and Cretaceous and 5–12 m/my in the mid-Cretaceous interval with volcaniclastic input. Overlying abyssal red clays of the Cenozoic section at both sites show rates of <1 m/my, which are typical of the NW Pacific in the Cenozoic (Moore et al., 2015). Therefore, we concluded that pelagic sedimentation rates calibrated by ocean drilling in the NW Pacific and West Philippine Basin are in good agreement with the predictions of the Lower Cretaceous age for the Huatung Basin proposed by Deschamps et al. (2000), which was based on ages of dredged gabbros and of radiolarian cherts on Lanyu Island, plus modeling of magnetic anomalies. In contrast the alternative 30-Ma mid-Cenozoic age model, which is based largely on modeling of magnetic anomalies, yields a sedimentation rate of 25 m/my that is excessive for a deep oceanic pelagic sedimentation rate, although it would be compatible with hemipelagic sedimentation with significant volcaniclastic input.

The two post-15 Ma age models for the upper part of the lower Huatung Basin sequence predict similar sedimentation rates of 51–60 m/my (Table 2, b), which are reasonable for pelagic sedimentation with an input of local volcanic source, particularly with the observed chaotic seismic facies 6 mass-transport deposits. ODP site 436 east of the Japan Trench gives a volcaniclastic hemipelagic rate of 22.5 m/my for the last 16 Ma and a rate of 0.4–0.8 m/my for underlying Cenozoic and Cretaceous pelagic clay and chert showing sheet-drape seismic facies (Moore et al., 2015; Nakamura et al., 2013). Similarly, the upper Miocene to Pleistocene uppermost part of IODP site 1149 shows upward increasing rates of 13–34 m/my reflecting Izu-Bonin arc input of volcanic ash within diatom and radiolarian clay. Both of these drilling sites are separated from the arc by an intervening trench, in contrast with the Huatung Basin setting, but they illustrate the effect of typical pelagic oceanic sections approaching an arc.

7.1.2. Middle Seismic Sequence: Initiation of the Chimei Canyon-Fan System

The middle seismic sequence marks a profound change in the Huatung Basin which we interpret as the onset of Taiwan-derived orogenic deposition. The seismic sequence boundary *Y* at the base of the middle sequence marks an abrupt change in basinwide reflection character from transparent wedge-shaped seismic facies (seismic facies 2) above to higher amplitude reflections of the pelagic sheet-drape seismic facies below (Figures 8, 9, and S1). The mean seismic velocity increases from 2.8 to 2.9 km/s in the middle sequence to 3.5 km/s in the upper part of the lower sequence. The middle transparent seismic sequence appears to record the initial development of a transport pathway for Taiwan orogenic sediments across the forearc basin and Luzon Arc and into the deep Huatung Basin, based on the observed isopach, downlap, and facies distribution, which is consistent with a distal submarine fan derived from the west (Figures 13c and 13d). In seismic sections perpendicular to the mountain belt, the external shape of the middle sequence is wedge-shaped, thinning markedly toward the eastern Huatung Basin (Figures 14 and S6) and appears mound shaped in orthogonal sections (Figures 8, 10, and S1), consistent with a distal fan interpretation.

These observations point to a localized transport pathway coming from the west passing through a gap or spill point in the arc from the forearc basin, perhaps similar to the present-day Taitung Canyon pathway (Figure 2). If the elevation of the spill point is high, then large filling of the forearc basin is required before the Chimei Fan can develop on the Huatung Basin, but if the spill point is low like the Taitung Canyon, then the base of the middle seismic sequence will be older. Since there is no direct determination of ages in the Huatung Basin, we present two plausible age models for Chimei Fan development (Table 2, a), which correspond to earlier and later spillover into the Huatung Basin, discussed below. Our preferred model correlates the age of the middle seismic sequence with the time of the most rapid filling of the forearc basin to the west (1–2 Ma, Figure 5), with the upper seismic sequence recording a shift of depocenter to east of the arc, with the termination of forearc basin deposition (0–1 Ma, Figure 5). The alternative model correlates the base of the middle sequence with the first arrival of Taiwan-derived sediments in the forearc basin (~4 Ma, Figure 5; Chi et al., 1981; Teng, 1979) and correlates the top of the middle sequence with the acceleration of sedimentation in the forearc basin (~2 Ma, Figure 5).

In the middle seismic sequence, we do not observe seismic facies of proximal submarine canyon and fan in the Huatung Basin, whereas in the Coastal Range to the west, the 1- to 1.6-Ma Chimei conglomerate member of the Paliwan Formation just north of the Hsiukuluan River (Figure 4) consists of coarse marine conglomerate and associated sand-rich to mud-rich turbidites and possible storm deposits (Chi et al., 1981; Dorsey & Lundberg, 1988). Hence, we suggest that the proximal initial Chimei Canyon and Fan has been uplifted and exposed onshore as the Chimei conglomerate (Figures 4 and 17). We emphasize that there has been ~60-km shortening of the currently 40-km-wide thrust belt in the last ~1 Ma (Figure 17); thus, the distal fan of the middle sequence, which is east of the frontal thrust, was ~100–160 km east of the proximal Chimei conglomerate channel and fan in the forearc basin, which was deposited during the most rapid infilling of the forearc basin (3–7.4 km/my, Figure 5).

According to our preferred age model (Table 2, a), the proximal facies of the western Coastal Range would be coeval with the distal fan of the transparent middle seismic sequence ~100–160 km to the east. The middle sequence distal fan sedimentation rate is ~470 m/my for the preferred 1- to 2-Ma model, which is about an order of magnitude less than the rate in the Coastal Range (3,700–7,380 m/my), which seems plausible given the proximal rapid infilling of the linear forearc basin in the west in contrast to unconfined basin plain 100–160 km to the east. The alternative age model, which correlates the middle seismic sequence with the initial 2- to 4-Ma Taiwan-derived sediments of the forearc basin, predicts a rate of 130–400 m/my for the distal fan which is likely too fast compared with the 480–629 m/my of forearc basin rate in the northern Coastal Range 100–160 km to the west.

7.1.3. Upper Seismic Sequence: Post-1 Ma Growth of Chimei Canyon-Fan System

In the upper seismic sequence, the hummocky, high-amplitude onlapping-fill seismic facies (facies 5) in the Chimei deep-sea valley is interpreted as sand lobe and channel seismic facies (Figure 9), and the low-amplitude, high-continuous divergent seismic facies (facies 3) in the Chimei Fan is interpreted as levee seismic facies (Figure 9). The channel and levee seismic facies comprise the Chimei Fan in the upper sequence, whose scale is much larger than the Chimei Fan in the middle sequence (Figures 10 and 11), recording a major expansion of the Huatung Basin depocenter.

We suggest that the offshore upper sequence records deposition of the Chimei Fan during post-1 Ma uplift of the Coastal Range and carving of the antecedent Hsiukuluan River gorge. Before 1 Ma, most sediment eroded from the Central Range was trapped in the forearc basin depocenter with sedimentation rates reaching 3,000–7,400 m/my (Figure 5), which was terminated by the imbricate thrusting of the Coastal Range thrust belt (Figure 17). As a result, all sediment from the Central Range started to pass directly from the narrow Longitudinal Valley, through the Hsiukuluan River gorge, and into the offshore Chimei Canyon and Fan. Hence, the Chimei Fan grew rapidly after ~1 Ma as it became the principal and then the sole depocenter.

To estimate the age of the upper seismic sequence, we apply indirect constraints from seismic facies analysis, and by comparing the erosion rates in the source area (Central Range) with deposition rates and sediment volumes in the Coastal Range and Chimei Fan (the "sinks"). In the Coastal Range, there are no marine stratigraphic records younger than ~1 Ma, but an unconformity separates the early Pleistocene marine strata and minor late Pleistocene nonmarine strata (Chi et al., 1981; Chen & Wang, 1996). We speculate that the depocenter shifted offshore after 1 Ma due to uplift of the Coastal Range and destruction of the arc and

forearc basin by deformation. The upper seismic sequence is 1.2 km thick on average. Assuming the seismic sequence boundary *X* (base of upper sequence) to be 1 Ma, the depositional rate is 1,200 m/my This rate is comparable to an ~3,000-year depositional rate measured in a shallow marine core on the Changping High offshore eastern Taiwan (1.09 mm/yr) (Lallemand et al., 2016).

We compare the sediment volume of the Chimei Canyon-Fan to the sediment flux of the present Hsiukuluan River catchment (Table 3). The erosion rate is 4–5 mm/yr at the eastern side of the Central Range (Derrieux et al., 2014; Fellin et al., 2017; Lundberg & Dorsey, 1990). Assuming an erosion rate of 4–5 km/my, we estimate that 7,564–9,455 km^3 of rock has been eroded from a catchment of the size of the current Hsiukuluan River in the past ~1 Ma. The sediment volume of the Chimei Canyon-Fan is around 8,970 km^3, which is the sum of the volume of canyon wall strata, Chimei Fan, and the frontal part of the Ryukyu accretionary wedge close to the Chimei Fan which we believe were formed by accreting Chimei Fan sediment onto the Ryukyu accretionary wedge (Figures 11a and 11b). We convert the preserved volume of sediment to equivalent rock volume of 7,176–8,073 km^3 for the Chimei Canyon-Fan system (Table 3), which is comparable to the 7,564- to 9,455-km^3 eroded volume of rock of the present Hsiukuluan River catchment in 1 Ma (Table 3). Therefore, an estimate of $\lesssim$1 Ma for the upper sequence is plausible from a mass balance consideration.

This estimate of ~1 Ma for the shift of the principal depocenter from onshore to offshore is also consistent with the structural shortening along the transport pathway shown in Figure 17. The total shortening is $\gtrsim$62 km which at the current geodetic shortening rate of ~60 mm/yr gives a bit more than ~1 Ma for the age of destruction of the arc and forearc basin at the latitude of Chimei Canyon (section 6.4). The beginning of thrusting of the Chimei Canyon thrust is close to the top of the middle seismic sequence based on growth strata, which is consistent with the ~1-Ma age assignment for that boundary (section 6.1).

Finally, in Table 2 (b), we compare our (1) preferred age (0–1 Ma) model for the upper seismic sequence, which is correlated with the end of forearc basin deposition and the shift in depocenter to east of the Luzon Arc, with (2) an alternative (0–2 Ma) model that correlates the start of the upper sequence with the acceleration of deposition ~2 Ma in the forearc basin (Figure 5; Table 2, a). According to this model, there is a more extended overlap in age between the record of orogenic deposition in the Coastal Range (1–4 Ma) and the time of deposition of the middle and upper seismic sequences in the Huatung Basin (0–4 Ma). The predicted average sedimentation rate for the preferred model in the upper sequence is ~1,200 m/my, but 600 m/my in the alternative model (Table 2, a) which does not agree with the source-to-sink mass balance (Table 3) or the history of deformation beginning ~1 Ma onshore and just before the top of the middle sequence offshore based on growth strata. For this, alternative model to be viable would require a more elaborate time varying source-to-sink mass balance and a more complex deformation history, which cannot be evaluated with present constraints.

7.2. Tectonic Control of the Chimei Canyon

The Chimei Canyon is a wedge-top system that is confined to the Offshore East Taiwan thrust belt. The distal terminus of the canyon coincides with the Chimei Canyon frontal thrust and the steep headwall at the top of the canyon coincides with the syncline marking the beginning of the west-vergent Coastal Range thrust belt (Figure 17). Several observations suggest that Chimei Canyon may be controlled by structural uplift rate and contrasts in erodibility of stratigraphy. The maximum uplift of the pre-orogenic Huatung Basin sequence in the Chimei Canyon thrust is 2.5–2.7 km near the toe of the thrust (Figure 13), with a relatively modest ~2.5 mm/yr of uplift rate since ~1-Ma reflecting modest fault dip relative to the 20 mm/yr of shortening rate (Figure 14). In contrast, the Chimei Canyon has not propagated headward into the Coastal Range thrust belt where uplift rates are much higher (6–20 mm/yr; Chen et al., 2020; Hsieh et al., 2004; Liew et al., 1993; Shyu et al., 2006; Yamaguchi & Ota, 2004) reflecting steeper faults and ~40 mm/yr of combined shortening rate. In addition, most of the Coastal Range thrusts contain Miocene Tuluanshan Volcanics, which are more resistant to erosion, forming 0.5–1 km of relief in the vicinity of the Hsiukuluan River gorge (Figure 4). In contrast, the Chimei Canyon is cut largely in the more erodable syn-orogenic sequences, with only modest erosion of the pre-orogenic Huatung Basin sequence to judge from the similar areas of relief of pre-orogenic strata in Figures 14 and 15. The 1- to 1.6-Ma paleo-Chimei Canyon fill exposed on land is confined to the more erodible Paliwan Formation, which is considered a submarine fan deposit of the forearc basin (Chen, 2016; Dorsey & Lundberg, 1988, 1989) (Figure 4).

The >20-km-long Chimei Canyon thrust sheet south of Chimei Canyon (Figure 14) has remained intact in spite of complex fault geometry because it has been stabilized to supercritical geometry by the deposition of the overlying wedge-shaped Chimei Fan, which has increased the taper to ~8° from its initial ~2° taper in pre-fan strata (section 6.2). In contrast, the thrust belt in Chimei Canyon (Figure 15) has undergone erosion causing it to develop a classic imbricated critical taper structure (4°) that apparently controls the regional surface slope of the canyon (Figure 7c). Therefore, active fan and canyon surface processes have made an observable impact on the mechanics of the underlying Chimei Canyon thrust system.

8. Conclusion

This is the first detailed analysis of the record and nature of arc-continent collision in a portion of offshore eastern Taiwan, which is on the rapidly deforming overriding Philippine Sea Plate that has undergone ~60-km shortening in the last 1 Ma. We have presented the morphology, seismic stratigraphy, and structure of the wedge-top Chimei Canyon-Fan system based on bathymetry and seismic reflection profile data, including an integration with onshore stratigraphy and structure of the deformed arc and forearc basin of the Coastal Range (Figures 4 and 17). The Chimei Canyon shows a very distinct U-shape (box shape) cross-sectional morphology (Figure 1), 5–14 km wide and very smooth bottom (Figures 3, 4, and 7). The Chimei Canyon is entirely confined to the east-vergent Offshore East Taiwan thrust belt, incised into wedge-top submarine fan deposits, which have uplifted up to 2.5–2.7 km, with the frontal thrust marking the foot of the canyon. The steep canyon headwall (~20°) marks the synclinal edge of the west-vergent onshore Coastal Range thrust belt, which has 2–8 times higher uplift rates and includes arc volcanic rocks that are resistant to erosion (Figure 17). The Chimei submarine fan exists in two parts: the proximal and uplifting wedge-top fan into which the Chimei Canyon is incised (Figure 16) and a more distal fan east of the thrust belt that is also incised, but without uplift, and eroded by a complex submarine valley system with the northern part of the fan largely removed (Figures 3, 10, and 11). The entire system is marked by aggradation followed by incision within the last ~1 Ma.

The Chimei Canyon is sourced by the Hsiukuluan River catchment, the only river that cuts completely across the Coastal Range thrust belt; thus, the canyon receives sediments from both the Central Range and Coastal Range (Figure 3a). We analyze the Chimei Canyon and Fan in the context of the entire source-to-sink system, which has undergone ~60 km of shortening in the last 1 Ma. The onshore Coastal Range thrust belt is composed of thrust sheets of the deformed arc and forearc basin strata, whereas the Chimei Canyon and Fan overlie oceanic crust of the Huatung Basin east of the Luzon Arc. The Taiwan-derived forearc and supra-arc strata of the Coastal Range are almost entirely older than ~1 Ma and represent the main Taiwan-derived depocenter during 1–4 Ma (Figure 5). After ~1 Ma, the depocenter shifted entirely to the offshore Chimei Canyon-Fan, east of the Luzon Arc. A 1- to 1.6-Ma paleo-Chimei Canyon channel complex is uplifted and exposed in the Coastal Range adjacent to the Hsukuluan River and shows transport parallel to the present offshore Chimei Canyon (Figure 4), suggesting that the present transport pathway may have been long lived and antecedent to thrusting, which is consistent with offshore thickness and facies distributions pointing to such a paleo-pathway (Figures 12c and 12d). Our analysis concludes that the strata of the Chimei Canyon-Fan may be considered distal (<2 Ma) and in-part younger (<1 Ma) equivalents of Taiwan-derived orogenic strata in the Coastal Range.

The sedimentary strata of the Huatung Basin are subdivided into three seismic sequences based on seismic facies analysis, with their ages interpreted by comparison of sedimentation rates and facies between the Coastal Range (Figure 5) and the offshore Chimei Fan (Table 2), and comparison of sediment volume of the Chimei Fan and with sediment fluxes of the Hsiukuluan River drainage (Table 3). The lowest seismic sequence is dominated by pelagic seismic facies that we interpret as the Early Cretaceous to Neogene pre-collisional sequence deposited on the stable Huatung Basin oceanic crust (Figure 8). The uppermost lower sequence shows the addition of chaotic seismic facies (Figure S1) that may be derived from the Luzon Arc after it was established ~15 Ma. The base of the middle seismic sequence marks the onset of organized orogenic source-to-sink transport from the mountain belt, across a spill point in the arc and into the deep Huatung Basin, triggered by filling of the forearc basin to a critical height. The middle and upper seismic sequences are syn-collisional sequences that show high energy seismic facies (Figures 8–11) and thickness variations (Figure 12) characteristic of submarine fan and channel environments. We propose a model

for the development of the Chimei Canyon-Fan in which Taiwan-derived sediment was largely trapped in the Luzon Trough forearc basin prior to ~2 Ma (Figure 5). The distal Chimei Canyon and Fan were initiated as the middle seismic sequence ~2 Ma when the adjacent Taiwan mountain belt was uplifting rapidly and the forearc basin strata of the Coastal Range were being deposited at rates of 2–7 km/my. No marine strata exist in the Coastal Range younger than ~1 Ma, indicating termination of the forearc depocenter. The Chimei Fan grew most rapidly in the upper seismic sequence, which we interpret to be deposited largely after ~1 Ma, reflecting a shift in dominant depocenter along the paleo-Hsiukuluanchi/Chimei Canyon transport pathway from the forearc basin to the Huatung Basin, caused by the uplift of the Coastal Range thrust belt. The Offshore East Taiwan thrust belt also grew at this time, resulting in a wedge-top pathway for the sediments coming from the Central Range (Figures 4, 5, and 17). The total shortening of the combined onshore-offshore thrust belts is >62 km, which at the present geodetic shortening rate of ~60 mm/yr is consistent with ~1 Ma of deformation for the observed structures, with ~20 mm/yr in the offshore and ~40 mm/yr onshore.

Data Availability Statement

The seismic and gridded bathymetry data are stored in the Ocean Data Bank of MOST (http://www.odb.ntu.edu.tw/en/). Most seismic profile data were processed at the Seismic Exploration Lab, Institute of Oceanography NTU. ProMAX seismic data processing software was used to obtain poststack time-migrated profiles. EMERSON Paradigm ECHOS and GeoDepth seismic data processing software was used to generate two pre-stack depth-migrated profiles. Kingdom software was used for displaying seismic reflection profile. GMT was used for geographic plots. StructureSolver software was used for restoration and measurement of shortening distances. Paradigm software was donated by EMERSON and StructureSolver software by Nunns and Rogan LLC to University of Houston.

Acknowledgments

This study started as an undergraduate summer program funded by the National Science Council (NSC, now Ministry of Science and Technology) grant 100-3113-M-002-002 and later developed to a graduate program at the Institute of Oceanography, National Taiwan University (NTU), and as a PhD project at the University of Houston. Yu-Huan Hsieh was an MS student at Institute of Oceanography NTU funded by the NSC grant 102-3113-P-002-036 to Char-Shine Liu, a research assistant at Department of Geoscience NTU funded by Ministry of Science and Technology (MOST) grants 103-2116-M-002-030 and 104-2116-M-002-028 to John Suppe, a research assistant at Ocean Center NTU funded by MOST grant 106-3113-M-002-004 to Char-Shine Liu, and a PhD student at the Department of Earth and Atmospheric Sciences UH funded by University of Houston and the State of Texas GURI Research Initiative to John Suppe. We thank the captains, crew, and science staff of the R/Vs *Ocean Researcher I, Maurice Ewing* (TAICRUST project) and *Marcus G. Langseth* (TAIGER project) for collecting the multichannel seismic data used in this study, and R/V *l'Atalant* (ACT cruise) for collecting the swath bathymetry data in the study area. The TAICRUST and TAIGER projects were Taiwan-US collaborative projects funded by MOST in Taiwan and NSF in the United States. The ACT cruise was part of the Taiwan-France collaborative project supported by INSU-CNRS in France and NSC in Taiwan. We would like to acknowledge INSU-CNRS and IFREMER for their supports in funding the ACT cruise and related research to Serge Lallemand. We are grateful to Ocean Center and Institute of Oceanography, NTU for providing the bathymetric and seismic data and technical support for this study. Ho-Han Hsu, Min-Han Chuang, and Ying-Cheng Yeh helped to prepare the bathymetry and seismic data. The data provider is the Marine Academic Database of the Ministry of Science and Technology and the Seismic Exploration Lab, Institute of Oceanography, National Taiwan University. We especially thank many colleagues for helpful discussions, including Rebecca Dorsey, Louis Teng, Chi-Yue Huang, Wen-Shan Chen, Andrew Tien-Shun Lin, Wu-Cheng Chi, and Hao Kuo-Chen. Finally, we are grateful to the two anonymous reviewers for improving our manuscript.

References

Alam, M., Alam, M. M., Curray, J. R., Chowdhury, M. L. R., & Gani, M. R. (2003). An overview of the sedimentary geology of the Bengal Basin in relation to the regional tectonic framework and basin-fill history. *Sedimentary Geology*, *155*(3–4), 179–208. https://doi.org/10.1016/s0037-0738(02)00180-x

Angelier, J., Barrier, E., & Chu, H. T. (1986). Plate collision and paleostress trajectories in a fold thrust belt—The foothills of Taiwan. *Tectonophysics*, *125*(1–3), 161–178. https://doi.org/10.1016/0040-1951(86)90012-0

Argus, D. F., Gordon, R. G., & DeMets, C. (2011). Geologically current motion of 56 plates relative to the no-net-rotation reference frame. *Geochemistry, Geophysics, Geosystems*, *12*, Q11001. https://doi.org/10.1029/2011GC003751

Barrier, E., & Angelier, J. (1986). Active collision in eastern Taiwan: The Coastal Range. *Tectonophysics*, *125*(1–3), 39–72. https://doi.org/10.1016/0040-1951(86)90006-5

Bernhardt, A., Melnick, D., Jara-Munoz, J., Argandona, B., Gonzalez, J., & Strecker, M. R. (2015). Controls on submarine canyon activity during sea-level highstands: The Biobio Canyon System offshore Chile. *Geosphere*, *11*(4), 1226–1255. https://doi.org/10.1130/ges01063.1

Biq, C. (1972). Dual-trench structure in the Taiwan-Luzon Region. *Proceedings of the Geological Society of China*, *15*, 65–75.

Boutelier, D., Chemenda, A., & Burg, J. P. (2003). Subduction versus accretion of intra-oceanic volcanic arcs: Insight from thermo-mechanical analogue experiments. *Earth and Planetary Science Letters*, *212*(1–2), 31–45. https://doi.org/10.1016/s0012-821x(03)00239-5

Bowin, C., Lu, R. S., Lee, C. S., & Schouten, H. (1978). Plate convergence and accretion in Taiwan-Luzon Region. *AAPG Bulletin*, *62*(9), 1645–1672.

Byrne, T., Chan, Y. C., Rau, R. J., Lu, C. Y., Lee, Y. H., & Wang, Y. J. (2011). The arc-continent collision in Taiwan. In D. Brown & P. D. Ryan (Eds.), *Arc-continent collision, frontiers in Earth sciences* (pp. 213–245). Berlin Heidelberg: Springer-Verlag. https://doi.org/10.1007/978-3-540-88558-0_8

Carlson, P. R., & Karl, H. A. (1988). Development of large submarine canyons in the Bering Sea, indicated by morphologic, seismic, and sedimentologic characteristics. *Geological Society of America Bulletin*, *100*(10), 1594–1615. https://doi.org/10.1130/0016-7606(1988)100<1594:dolsci>2.3.co;2

Chai, B. H. T. (1972). Structure and tectonic evolution of Taiwan. *American Journal of Science*, *272*(5), 389–422. https://doi.org/10.2475/ajs.272.5.389

Chemenda, A. I., Hurpin, D., Tang, J. C., Stephan, J. F., & Buffet, G. (2001). Impact of arc-continent collision on the conditions of burial and exhumation of UHP/LT rocks: Experimental and numerical modelling. *Tectonophysics*, *342*(1–2), 137–161. https://doi.org/10.1016/s0040-1951(01)00160-3

Chemenda, A. I., Yang, R. K., Hsieh, C. H., & Groholsky, A. L. (1997). Evolutionary model for the Taiwan collision based on physical modelling. *Tectonophysics*, *274*(1–3), 253–274. https://doi.org/10.1016/s0040-1951(97)00025-5

Chemenda, A. I., Yang, R. K., Stephan, J. F., Konstantinovskaya, E. A., & Ivanov, G. M. (2001). New results from physical modelling of arc-continent collision in Taiwan: Evolutionary model. *Tectonophysics*, *333*(1–2), 159–178. https://doi.org/10.1016/s0040-1951(00)00273-0

Chen, W. S. (2016). Geology of the Coastal Range (in Chinese). In W. S. Chen (Ed.), *Introduction to geology of Taiwan* (pp. 101–112). Taipei, Taiwan: Geological Society of Taiwan.

Chen, W. S., & Wang, Y. (1996). *Geology of the Coastal Range, eastern Taiwan, geological series of Taiwan (in Chinese)* (Vol. 7). Taipei, Taiwan: Central Geological Survey, MOEA.

Chen, W. S., Yang, C. Y., Chen, S. T., & Huang, Y. C. (2020). New insights into Holocene marine terrace development caused by seismic and aseismic faulting in the Coastal Range, eastern Taiwan. *Quaternary Science Reviews*, *240*. https://doi.org/10.1016/j.quascirev.2020.106369

Chi, W. R., Namson, J., & Suppe, J. (1981). Stratigraphic record of plate interactions in the Coastal Range of eastern Taiwan. *Memoir of Geological Society of China*, *4*, 155–194.

Chiang, C. S., & Yu, H. S. (2006). Morphotectonics and incision of the Kaoping submarine canyon, SW Taiwan orogenic wedge. *Geomorphology*, *80*(3–4), 199–213. https://doi.org/10.1016/j.geomorph.2006.02.008

Cohen, K. M., & Gibbard, P. L. (2019). Global chronostratigraphical correlation table for the last 2.7 million years, version 2019 QI-500. *Quaternary International*, *500*, 20–31. https://doi.org/10.1016/j.quaint.2019.03.009

Cook, K. L., Turowski, J. M., & Hovius, N. (2014). River gorge eradication by downstream sweep erosion. *Nature Geoscience*, *7*(9), 682–686. https://doi.org/10.1038/ngeo2224

Curray, J. R. (2014). The Bengal depositional system: From rift to orogeny. *Marine Geology*, *352*, 59–69. https://doi.org/10.1016/j.margeo.2014.02.001

Curray, J. R., Emmel, F. J., & Moore, D. G. (2003). The Bengal Fan: Morphology, geometry, stratigraphy, history and processes. *Marine and Petroleum Geology*, *19*(10), 1191–1223. https://doi.org/10.1016/s0264-8172(03)00035-7

Curray, J. R., & Moore, D. G. (1974). Sedimentary and tectonic processes in the Bengal deep-sea fan and geosyncline. In C. A. Burk & C. L. Drake (Eds.), *The geology of continental margins* (pp. 617–627). New York: Springer-Verlag. https://doi.org/10.1007/978-3-662-01141-6_45

Dadson, S., Hovius, N., Pegg, S., Dade, W. B., Horng, M. J., & Chen, H. (2005). Hyperpycnal river flows from an active mountain belt. *Journal of Geophysical Research*, *110*, F04016. https://doi.org/10.1029/2004jf000244

Dadson, S. J., Hovius, N., Chen, H., Dade, W. B., Hsieh, M.-L., Willett, S. D., et al. (2003). Links between erosion, runoff variability and seismicity in the Taiwan orogen. *Nature*, *426*(6967), 648–651. https://doi.org/10.1038/nature02150

Dadson, S. J., Hovius, N., Chen, H., Dade, W. B., Lin, J. C., Hsu, M. L., et al. (2004). Earthquake-triggered increase in sediment delivery from an active mountain belt. *Geology*, *32*(8), 733–736. https://doi.org/10.1130/g20639.1

Dahlen, F. A., & Suppe, J. (1988). Mechanics, growth, and erosion of mountain belts. In S. P. Clark, B. C. Burchfiel, J. Suppe (Eds.), *Processes in continental lithospheric deformation, Geological Society of America Special Papers* (Vol. 218, pp. 161–178). Boulder, Colorado: Geological Society of America. https://doi.org/10.1130/SPE218-p161

Davis, D., Suppe, J., & Dahlen, F. A. (1983). Mechanics of fold-and-thrust belts and accretionary wedges. *Journal of Geophysical Research*, *88*(NB2), 1153–1172. https://doi.org/10.1029/JB088iB02p01153

DeMets, C., Gordon, R. G., & Argus, D. F. (2010). Geologically current plate motions. *Geophysical Journal International*, *181*(1), 1–80. https://doi.org/10.1111/j.1365-246X.2009.04491.x

Derrieux, F., Siame, L. L., Bourlès, D. L., Chen, R. F., Braucher, R., Léanni, L., et al. (2014). How fast is the denudation of the Taiwan mountain belt? Perspectives from in situ cosmogenic Be-10. *Journal of Asian Earth Sciences*, *88*, 230–245. https://doi.org/10.1016/j.jseaes.2014.03.012

Deschamps, A., & Lallemand, S. (2002). The West Philippine Basin: An Eocene to early Oligocene back arc basin opened between two opposed subduction zones. *Journal of Geophysical Research*, *107*(B12), 2322. https://doi.org/10.1029/2001JB001706

Deschamps, A., Monié, P., Lallemand, S., Hsu, S. K., & Yeh, K. Y. (2000). Evidence for Early Cretaceous oceanic crust trapped in the Philippine Sea Plate. *Earth and Planetary Science Letters*, *179*(3–4), 503–516. https://doi.org/10.1016/s0012-821x(00)00136-9

Dimalanta, C. B., Faustino-Eslava, D. V., Gabo-Ratio, J. A. S., Marquez, E. J., Padrones, J. T., Payot, B. D., et al. (2020). Characterization of the proto-Philippine Sea Plate: Evidence from the emplaced oceanic lithospheric fragments along eastern Philippines. *Geoscience Frontiers*, *11*(1), 3–21. https://doi.org/10.1016/j.gsf.2019.01.005

Doo, W. B., Hsu, S. K., Yeh, Y. C., Tsai, C. H., & Chang, C. M. (2015). Age and tectonic evolution of the northwest corner of the West Philippine Basin. *Marine Geophysical Research*, *36*(2–3), 113–125. https://doi.org/10.1007/s11001-014-9234-8

Dorsey, R. (1985). Petrography of Neogene sandstones from the Coastal Range of eastern Taiwan: Response to arc-continent collision. *Petroleum Geology of Taiwan*, *21*, 187–215.

Dorsey, R., & Lundberg, N. (1989). Transport and depositional mechanisms for Lower Pleistocene submarine conglomerates, syn-collisional basin of eastern Taiwan. In R. Dorsey, (Ed.), Sedimentary and tectonic evolution of a Pliocene-Pleistocene collisional basin, Coastal Range of eastern Taiwan. (Ph.D. Thesis). Princeton University.

Dorsey, R. J. (1988). Provenance evolution and unroofing history of a modern arc-continent collision: Evidence from petrography of Plio-Pleistocene sandstones, eastern Taiwan. *Journal of Sedimentary Petrology*, *58*(2), 208–218. https://doi.org/10.1306/212f8d5a-2b24-11d7-8648000102c1865d

Dorsey, R. J. (1992). Collapse of the Luzon volcanic arc during onset of arc-continent collision: Evidence from a Miocene-Pliocene unconformity, eastern Taiwan. *Tectonics*, *11*(2), 177–191. https://doi.org/10.1029/91tc02463

Dorsey, R. J., & Lundberg, N. (1988). Lithofacies analysis and basin reconstruction of the Plio-Pleistocene collisional basin, Coastal Range of eastern Taiwan. *Acta Geologica Taiwanica*, *26*, 57–132.

Eakin, D. H., McIntosh, K. D., van Avendonk, H. J. A., & Lavier, L. (2015). New geophysical constraints on a failed subduction initiation: The structure and potential evolution of the Gagua ridge and Huatung Basin. *Geochemistry, Geophysics, Geosystems*, *16*, 380–400. https://doi.org/10.1002/2014gc005548

Fellin, M. G., Chen, C. Y., Willett, S. D., Christl, M., & Chen, Y. G. (2017). Erosion rates across space and timescales from a multi-proxy study of rivers of eastern Taiwan. *Global and Planetary Change*, *157*, 174–193. https://doi.org/10.1016/j.gloplacha.2017.07.012

Font, Y., Liu, C. S., Schnurle, P., & Lallemand, S. (2001). Constraints on backstop geometry of the southwest Ryukyu subduction based on reflection seismic data. *Tectonophysics*, *333*(1–2), 135–158. https://doi.org/10.1016/s0040-1951(00)00272-9

Fuller, C. W., Willett, S. D., & Brandon, M. T. (2006). Formation of forearc basins and their influence on subduction zone earthquakes. *Geology*, *34*(2), 65–68. https://doi.org/10.1130/g21828.1

Hayes, D. E., & Lewis, S. D. (1984). A geophysical-study of the Manila Trench, Luzon, Philippine. 1. Crustal structure, gravity, and regional tectonic evolution. *Journal of Geophysical Research*, *89*(B11), 9171–9195. https://doi.org/10.1029/JB089iB11p09171

Higuchi, Y., Yanagimoto, Y., Hoshi, K., Unou, S., Akiba, F., Tonoike, K., & Koda, K. (2007). Cenozoic stratigraphy and sedimentation history of the northern Philippine Sea based on multichannel seismic reflection data. *Island Arc*, *16*(3), 374–393. https://doi.org/10.1111/j.1440-1738.2007.00588.x

Hilde, T. W. C., & Lee, C. S. (1984). Origin and evolution of the West Philippine Basin: A new interpretation. *Tectonophysics*, *102*(1–4), 85–104. https://doi.org/10.1016/0040-1951(84)90009-x0

Ho, C. S. (1969). Geological significance of potassium-argon age of the Chimei igneous complex in eastern Taiwan. *Taiwan Geological Survey Bulletin*, *20*, 64–74.
Ho, C. S. (1979). Geologic and tectonic framework of Taiwan. *Memoir of the Geological Society of China*, *3*, 57–72.
Ho, C. S. (1986). A synthesis of the geologic evolution of Taiwan. *Tectonophysics*, *125*(1–3), 1–16. https://doi.org/10.1016/0040-1951(86)90004-1
Hsieh, M. L., Liew, P. M., & Hsu, M. Y. (2004). Holocene tectonic uplift on the Hua-tung coast, eastern Taiwan. *Quaternary International*, *115–116*, 47–70. https://doi.org/10.1016/s1040-6182(03)00096-x
Hsieh, M. L., & Rau, R. J. (2009). Late Holocene coseismic uplift on the Hua-tung coast, eastern Taiwan: Evidence from mass mortality of intertidal organisms. *Tectonophysics*, *474*(3–4), 595–609. https://doi.org/10.1016/j.tecto.2009.04.031
Hsiung, K. H., & Yu, H. S. (2011). Morpho-sedimentary evidence for a canyon-channel-trench interconnection along the Taiwan-Luzon plate margin, South China Sea. *Geo-Marine Letters*, *31*(4), 215–226. https://doi.org/10.1007/s00367-010-0226-7
Hsu, W. H., Byrne, T. B., Ouimet, W., Lee, Y. H., Chen, Y. G., van Soest, M., & Hodges, K. (2016). Pleistocene onset of rapid, punctuated exhumation in the eastern Central Range of the Taiwan orogenic belt. *Geology*, *44*(9), 719–722. https://doi.org/10.1130/g37914.1
Huang, C. Y., Chen, W. H., Wang, M. H., Lin, C. T., Yang, S., Li, X., et al. (2018). Juxtaposed sequence stratigraphy, temporal-spatial variations of sedimentation and development of modern-forming forearc Lichi Melange in North Luzon Trough forearc basin onshore and offshore eastern Taiwan: An overview. *Earth-Science Reviews*, *182*, 102–140. https://doi.org/10.1016/j.earscirev.2018.01.015
Huang, C. Y., Shyu, C. T., Lin, S. B., Lee, T. Q., & Sheu, D. D. (1992). Marine geology in the arc-continent collision zone off southeastern Taiwan: Implications for late Neogene evolution of the Coastal Range. *Marine Geology*, *107*(3), 183–212. https://doi.org/10.1016/0025-3227(92)90167-g
Huang, C. Y., Wu, W. Y., Chang, C. P., Tsao, S., Yuan, P. B., Lin, C. W., & Xia, K.-Y. (1997). Tectonic evolution of accretionary prism in the arc-continent collision terrane of Taiwan. *Tectonophysics*, *281*(1–2), 31–51. https://doi.org/10.1016/s0040-1951(97)00157-1
Huang, C. Y., Yuan, P. B., & Tsao, S. J. (2006). Temporal and spatial records of active arc-continent collision in Taiwan: A synthesis. *Geological Society of America Bulletin*, *118*(3–4), 274–288. https://doi.org/10.1130/b25527.1
Huang, H. H., Wu, Y. M., Song, X. D., Chang, C. H., Lee, S. J., Chang, T. M., & Hsieh, H. H. (2014). Joint Vp and Vs tomography of Taiwan: Implications for subduction-collision orogeny. *Earth and Planetary Science Letters*, *392*, 177–191. https://doi.org/10.1016/j.epsl.2014.02.026
Hung, H. T. (2010). Sedimentary environment and tectonic evolution in Southern Huatung Basin (Master Thesis). Retrieved from https://hdl.handle.net/11296/z8qtw4. Taiwan: National Taiwan University.
Ingersoll, R., Dickinson, W. R., & Graham, S. A. (2003). Remnant-ocean submarine fans: Largest sedimentary systems on Earth. In M. A. Chan & A. W. Archer (Eds.), *Extreme depositional environments: Mega end members in geologic time Geological Society of America Special Papers* (Vol. 370, pp. 191–208). Boulder, Colorado: Geological Society of America.
Ingle, J. C., Karig, D. E., & White, S. M. (1975). *Proceedings of the deep sea drilling project, initial reports* (Vol. 31). College Station, Texas: Ocean Drilling Program. https://doi.org/10.2973/dsdp.proc.31.1975
Klingelhoefer, F., Berthet, T., Lallemand, S., Schnurle, P., Lee, C. S., Liu, C. S., et al. (2012). *P*-wave velocity structure of the southern Ryukyu margin east of Taiwan: Results from the ACTS wide-angle seismic experiment. *Tectonophysics*, *578*, 50–62. https://doi.org/10.1016/j.tecto.2011.10.010
Kreemer, C., Blewitt, G., & Klein, E. C. (2014). A geodetic plate motion and global strain rate model. *Geochemistry, Geophysics, Geosystems*, *15*, 3849–3889. https://doi.org/10.1002/2014gc005407
Kuo, B. Y., Chi, W. C., Lin, C. R., Chang, E. T. Y., Collins, J., & Liu, C. S. (2009). Two-station measurement of Rayleigh-wave phase velocities for the Huatung Basin, the westernmost Philippine Sea, with OBS: Implications for regional tectonics. *Geophysical Journal International*, *179*(3), 1859–1869. https://doi.org/10.1111/j.1365-246X.2009.04391.x
Lai, L. S. H., Ng, T. W., & Teng, L. S. Y. (2018). Stratigraphic correlation of tuffaceous and psephitic strata in the Paliwan Formation, southern Coastal Range of eastern Taiwan (in Chinese). *Bulletin of Central Geological Survey MOEA*, *31*, 1–32.
Lallemand, S. (2016). Philippine Sea Plate inception, evolution, and consumption with special emphasis on the early stages of Izu-Bonin-Mariana subduction. *Progress in Earth and Planetary Science*, *3*(1), 26. https://doi.org/10.1186/s40645-016-0085-6
Lallemand, S., Lehu, R., Rétif, F., Hsu, S. K., Babonneau, N., Ratzov, G., et al. (2016). A similar to 3000 years-old sequence of extreme events revealed by marine and shore deposits east of Taiwan. *Tectonophysics*, *692*, 325–341. https://doi.org/10.1016/j.tecto.2015.11.001
Lallemand, S., Liu, C. S., Angelier, J., Collot, J. Y., Deffontaines, B., Dominguez, S., et al. (1997). Swath bathymetry reveals active arc-continent collision near Taiwan. *EOS, Transactions American Geophysical Union (0096–3941)*, *78*(17), 173–175. https://doi.org/10.1029/97EO00116
Lancelot, Y., Fisher, A., Rabinowitz, P. D., Meyer, A. W., & Garrison, L. E. (1990). *Proceedings of the ocean drilling program, initial reports* (Vol. 129). College Station, Texas: Ocean Drilling Program. https://doi.org/10.2973/odp.proc.ir.129.1990
Le Béon, M., Marc, O., Suppe, J., Huang, M. H., Huang, S. T., & Chen, W. S. (2019). Structure and deformation history of the rapidly growing Tainan anticline at the deformation front of the Taiwan mountain belt. *Tectonics*, *38*, 3311–3334. https://doi.org/10.1029/2019tc005510
Lehu, R., Lallemand, S., Hsu, S. K., Babonneau, N., Ratzov, G., Lin, A. T., & Dezileau, L. (2015). Deep-sea sedimentation offshore eastern Taiwan: Facies and processes characterization. *Marine Geology*, *369*, 1–18. https://doi.org/10.1016/j.margeo.2015.05.013
Lehu, R., Lallemand, S., Ratzov, G., Babonneau, N., Hsu, S. K., Lin, A. T., & Dezileau, L. (2016). An attempt to reconstruct 2700 years of seismicity using deep-sea turbidites offshore eastern Taiwan. *Tectonophysics*, *692*, 309–324. https://doi.org/10.1016/j.tecto.2016.04.030
Liew, P. M., Pirazzoli, P. A., Hsieh, M. L., Arnold, M., Barusseau, J. P., Fontugne, M., & Giresse, P. (1993). Holocene tectonic uplift deduced from elevated shorelines, eastern Coastal Range of Taiwan. *Tectonophysics*, *222*(1), 55–68. https://doi.org/10.1016/0040-1951(93)90189-q
Lin, S. H. (2010). *Structural characteristics along the eastern flank of the northern Luzon Arc* (Master Thesis). Retrieved from https://hdl.handle.net/11296/f2zp46. Taiwan: National Taiwan University.
Liu, C. S., Deffontaines, B., Lu, C. Y., & Lallemand, S. (2004). Deformation patterns of an accretionary wedge in the transition zone from subduction to collision offshore southwestern Taiwan. *Marine Geophysical Researches*, *25*(1–2), 123–137. https://doi.org/10.1007/s11001-005-0738-0
Liu, C. S., Liu, S. Y., Kuo, B. Y., Lundberg, N., & Reed, D. L. (1992). Characteristics of the gravity and magnetic anomalies off southern Taiwan. *Acta Geologica Taiwanica*, *30*, 123–130.

Liu, C. S., Liu, S. Y., Lallemand, S. E., Lundberg, N., & Reed, D. L. (1998). Digital elevation model offshore Taiwan and its tectonic implications. *Terrestrial, Atmospheric and Oceanic Sciences*, *9*(4), 705–738. https://doi.org/10.3319/tao.1998.9.4.705(taicrust)

Liu, C. S., Schnürle, P., Lallemand, S. E., & Reed, D. L. (1997a). Crustal structures of the Philippine Sea plate near Taiwan. Paper presented at the Tectonics of East Asia (TEA) International Conference, Chung-Li, Taiwan.

Liu, C. S., Schnürle, P., Lallemand, S. E., & Reed, D. L. (1997b). TAICRUST and deep seismic imaging of western end of the Ryukyu arc-trench system. In *Deep sea research in subduction zone, spreading centers and backarc basin, JAMSTEC Journal of Deep Sea Research Special Volume* (pp. 39–45). Yokosuka, Japan: Japan Agency for Marine-Earth Science and Technology.

Liu, Y. D., Tan, X., Ye, Y., Zhou, C., Lu, R., Murphy, M. A., et al. (2020). Role of erosion in creating thrust recesses in a critical-taper wedge: An example from eastern Tibet. *Earth and Planetary Science Letters*, *540*, 1–12. https://doi.org/10.1016/j.epsl.2020.116270

Lopez, M. (2001). Architecture and depositional pattern of the Quaternary deep-sea fan of the Amazon. *Marine and Petroleum Geology*, *18*(4), 479–486. https://doi.org/10.1016/s0264-8172(00)00071-4

Lundberg, N., & Dorsey, R. J. (1990). Rapid Quaternary emergence, uplift, and denudation of the Coastal Range, eastern Taiwan. *Geology*, *18*(7), 638–641. https://doi.org/10.1130/0091-7613(1990)018<0638:rqeuad>2.3.co;2

Malavieille, J., Lallemand, S. E., & ACT (active collision in Taiwan) cruise scientific team. (1997). Arc-continent collision south-east of Taiwan: preliminary results of the ACT cruise. Paper presented at the the Abstract in Terra Nova 9, suppl. on EGU 9 Conference, Strasbourg.

Malavieille, J., Lallemand, S. E., Dominguez, S., Deschamps, A., Lu, C. Y., Liu, C. S., et al. (2002). Arc-continent collision in Taiwan: New marine observations and tectonic evolution. In T. Byrne & C. S. Liu (Eds.), *Geology and geophysics of an arc–continent collision, Geological Society of America Special Paper* (Vol. 358, pp. 189–213). Boulder, Colorado: Geological Society of America.

Mitchum, R. M. (1985). Seismic stratigraphic expression of submarine fans. In O. R. Berg, & D. G. Woolverton (Eds.), *Seismic stratigraphy II: An integrated approach to hydrocarbon exploration, AAPG Memoir* (Vol. 39, pp. 117–136). Tulsa, Oklahoma, U. S. A.: American Association of Petroleum Geologists.

Mitchum, R. M., & Vail, P. R. (1977). Seismic stratigraphy and global changes of sea level, part 7: Seismic stratigraphic interpretation procedure. In C. E. Payton (Ed.), *Seismic stratigraphy—Applications to hydrocarbon exploration, AAPG Memoir* (Vol. 26, pp. 135–143). Tulsa, Oklahoma, U. S. A.: Association of Petroleum Geologists.

Mitchum, R. M., Vail, P. R., & Sangree, J. B. (1977). Seismic stratigraphy and global changes of sea level, part 6: Stratigraphic interpretation of seismic reflection patterns in depositional sequences. In C. E. Payton (Ed.), *Seismic stratigraphy—Applications to hydrocarbon, exploration, AAPG Memoir* (Vol. 26, pp. 117–133). Tulsa, Oklahoma, U. S. A.: American Association of Petroleum Geologists.

Mitchum, R. M., Vail, P. R., & Thompson, S. (1977). Seismic stratigraphy and global changes of sea level, part 2: The depositional sequence as a basic unit for stratigraphic analysis. In C. E. Payton (Ed.), *Seismic stratigraphy—Applications to hydrocarbon exploration, AAPG Memoir* (Vol. 26, pp. 53–62). Tulsa, Oklahoma, U. S. A.: American Association of Petroleum Geologists.

Moore, J. C., Plank, T. A., Chester, F. M., Polissar, P. J., & Savage, H. M. (2015). Sediment provenance and controls on slip propagation: Lessons learned from the 2011 Tohoku and other great earthquakes of the subducting northwest Pacific Plate. *Geosphere*, *11*(3), 533–541. https://doi.org/10.1130/ges01099.1

Mount, V. S., Suppe, J., & Hook, S. C. (1990). A forward modeling strategy for balancing cross-sections. *AAPG Bulletin-American Association of Petroleum Geologists*, *74*(5), 521–531.

Mountjoy, J. J., Howarth, J. D., Orpin, A. R., Barnes, P. M., Bowden, D. A., Rowden, A. A., et al. (2018). Earthquakes drive large-scale submarine canyon development and sediment supply to deep-ocean basins. *Science Advances*, *4*(3), 8. https://doi.org/10.1126/sciadv.aar3748

Nakamura, Y., Kodaira, S., Miura, S., Regalla, C., & Takahashi, N. (2013). High-resolution seismic imaging in the Japan Trench axis area off Miyagi, northeastern Japan. *Geophysical Research Letters*, *40*, 1713–1718. https://doi.org/10.1002/grl.50364

Normark, W. R., & Carlson, P. R. (2003). Giant submarine canyons: Is size any clue to their importance in the rock record? In M. A. Chan & A. W. Archer (Eds.), *Extreme depositional environments: Mega end members in geologic time Geological Society of America Special Papers* (Vol. 370, pp. 175–190). Boulder, Colorado: Geological Society of America.

Normark, W. R., Piper, D. J. W., & Hiscott, R. N. (1998). Sea level controls on the textural characteristics and depositional architecture of the Hueneme and associated submarine fan systems, Santa Monica Basin, California. *Sedimentology*, *45*(1), 53–70. https://doi.org/10.1046/j.1365-3091.1998.00139.x

Park, J. O., Tokuyama, H., Shinohara, M., Suyehiro, K., & Taira, K. (1998). Seismic record of tectonic evolution and backarc rifting in the southern Ryukyu Island arc system. *Tectonophysics*, *294*(1–2), 21–42. https://doi.org/10.1016/s0040-1951(98)00150-4

Plank, T., Ludden, J. N., Escutia, C., & Party, S. S. (2000). *Proceedings of the ocean drilling program, initial reports* (Vol. 185). College Station, Texas: Ocean Drilling Program. https://doi.org/10.2973/odp.proc.ir.185.2000

Posamentier, H. W., & Kolla, V. (2003). Seismic geomorphology and stratigraphy of depositional elements in deep-water settings. *Journal of Sedimentary Research*, *73*(3), 367–388. https://doi.org/10.1306/111302730367

Reed, D. L., Lundberg, N., Liu, C. S., & Kuo, B. Y. (1992). Structural relations along the margins of the offshore Taiwan accretionary wedge: Implications for accretion and crustal kinematics. *Acta Geologica Taiwanica*, *30*, 105–122.

Rise, L., Bøe, R., Riis, F., Bellec, V. K., Laberg, J. S., Eidvin, T., et al. (2013). The Lofoten-Vesteralen continental margin, North Norway: Canyons and mass-movement activity. *Marine and Petroleum Geology*, *45*, 134–149. https://doi.org/10.1016/j.marpetgeo.2013.04.021

Sangree, J. B., & Widmier, J. M. (1977). Seismic stratigraphy and global changes of sea level, part 9: Seismic interpretation of clastic depositional facies. In C. E. Payton (Ed.), *Seismic stratigraphy—Applications to hydrocarbon exploration, AAPG Memoir* (Vol. 26, pp. 165–184). Tulsa, Oklahoma, U. S. A.: American Association of Petroleum Geologists.

Schnürle, P., Liu, C. S., Lallemand, S. E., & Reed, D. (1998). Structural controls of the Taitung Canyon in the Huatung Basin east of Taiwan. *Terrestrial, Atmospheric and Oceanic Sciences*, *9*(3), 453–472. https://doi.org/10.3319/tao.1998.9.3.453(taicrust)

Schwenk, T., Spieß, V., Breitzke, M., & Hübscher, C. (2005). The architecture and evolution of the Middle Bengal Fan in vicinity of the active channel-levee system imaged by high-resolution seismic data. *Marine and Petroleum Geology*, *22*(5), 637–656. https://doi.org/10.1016/j.marpetgeo.2005.01.007

Schwenk, T., Spieß, V., Hübscher, C., & Breitzke, M. (2003). Frequent channel avulsions within the active channel-levee system of the middle Bengal Fan—An exceptional channel-levee development derived from Parasound and Hydrosweep data. *Deep-Sea Research Part II-Topical Studies in Oceanography*, *50*(5), 1023–1045. https://doi.org/10.1016/s0967-0645(02)00618-5

Seno, T., Stein, S., & Gripp, A. E. (1993). A model for the motion of the Philippine Sea Plate consistent with NUVEL-1 and geological data. *Journal of Geophysical Research*, *98*(B10), 17,941–17,948. https://doi.org/10.1029/93jb00782

Shaw, J. H., Connors, C., & Suppe, J. (2004). *Seismic interpretation of contractional fault-related folds, an AAPG Atlas—Studies in geology* (Vol. 53). Tulsa, U.S.A.: American Association of Petroleum Geologists.

Shepard, F. P. (1973). *Submarine geology* (3rd ed.). New York: Harper & Row.

Shepard, F. P., & Buffington, E. C. (1968). La Jolla submarine fan-valley. *Marine Geology*, *6*(2), 107–143. https://doi.org/10.1016/0025-3227(68)90015-7

Shyu, J. B. H., Sieh, K., Avouac, J. P., Chen, W. S., & Chen, Y. G. (2006). Millennial slip rate of the Longitudinal Valley fault from river terraces: Implications for convergence across the active suture of eastern Taiwan. *Journal of Geophysical Research*, *111*, B08403. https://doi.org/10.1029/2005jb003971

Sibuet, J. C., Hsu, S. K., Le Pichon, X., Le Formal, J. P., Reed, D., Moore, G., & Liu, C. S. (2002). East Asia plate tectonics since 15 Ma: Constraints from the Taiwan region. *Tectonophysics*, *344*(1–2), 103–134. https://doi.org/10.1016/s0040-1951(01)00202-5

Stevenson, A. J., & Embley, R. (1987). Deep-sea fan bodies, terrigenous turbidite sedimentation, and petroleum geology, Gulf of Alaska. In D. W. Scholl, A. Grantz, J. G. Vedder (Eds.), *Geology and resource potential of the continental margin of western North America and adjacent ocean basins—Beaufort Sea to Baja California* (Vol. 6, pp. 503–522). Houston, Texas: Circum-Pacific Council for Energy and Mineral Resources, Earth Science Series.

Suppe, J. (1981). Mechanics of mountain building and metamorphism in Taiwan. *Memoir of Geological Society of China*, *4*, 67–89.

Suppe, J. (1983). Geometry and kinematics of fault-bend folding. *American Journal of Science*, *283*(7), 684–721. https://doi.org/10.2475/ajs.283.7.684

Suppe, J. (1984). Kinematics of arc-continent collision, flipping of subduction, and back-arc spreading near Taiwan. *Memoir of Geological Society of China*, *6*, 21–33.

Suppe, J. (1985). *Principles of Structural Geology: Englewood Cliffs*. New Jersey: Prentice-Hall, Inc.

Suppe, J. (1987). The active Taiwan mountain belt. In J. P. Schaer & J. Rogers (Eds.), *Anatomy of mountain chains* (pp. 277–293). Princeton, NJ: Princeton University Press.

Suppe, J. (2007). Absolute fault and crustal strength from wedge tapers. *Geology*, *35*(12), 1127–1130. https://doi.org/10.1130/g24053a.1

Suppe, J., Connors, C. D., & Zhang, Y. K. (2004). Shear fault-bend folding. In K. R. McClay (Ed.), *Thrust tectonics and hydrocarbon systems, AAPG Memoir* (Vol. 82, pp. 303–323). Tulsa, Oklahoma, U. S. A.: American Association of Petroleum Geologists.

Teng, L. S. (1979). Petrographical study of Neogene sandstones of the Coastal Range, eastern Taiwan. *Acta Geologica Taiwanica*, *20*, 129–155.

Teng, L. S. (1990). Geotectonic evolution of late Cenozoic arc-continent collision in Taiwan. *Tectonophysics*, *183*(1–4), 57–76. https://doi.org/10.1016/0040-1951(90)90188-e

Tsai, M. C., Yu, S. B., Shin, T. C., Kuo, K. W., Leu, P. L., Chang, C. H., & Ho, M. Y. (2015). Velocity field derived from Taiwan continuous GPS Array (2007-2013). *Terrestrial, Atmospheric and Oceanic Sciences*, *26*(5), 527–556. https://doi.org/10.3319/tao.2015.05.21.01(t)

Wang, T. K., Lin, S. F., Liu, C. S., & Wang, C. S. (2004). Crustal structure of the southernmost Ryukyu subduction zone: OBS, MCS and gravity modelling. *Geophysical Journal International*, *157*(1), 147–163. https://doi.org/10.1111/j.1365-246X.2004.02147.x

Wang, Y., & Chen, W. S. (1993). *Geologic map of eastern Coastal Range (scale 1:100,000)*. Taipei, Taiwan: Central Geological Survey, MOEA.

Wang, Y. J., & Yang, C. N. (1974). Geology and copper deposit of Chimei area, Coastal Range, Taiwan. *Proceedings of National Science Council*, *7*, 1–23.

Wu, J., Suppe, J., Lu, R. Q., & Kanda, R. (2016). Philippine Sea and East Asian Plate tectonics since 52 ma constrained by new subducted slab reconstruction methods. *Journal of Geophysical Research: Solid Earth*, *121*, 4670–4741. https://doi.org/10.1002/2016JB012923

Yamaguchi, M., & Ota, Y. (2004). Tectonic interpretations of Holocene marine terraces, east coast of Coastal Range, Taiwan. *Quaternary International*, *115-116*, 71–81. https://doi.org/10.1016/s1040-6182(03)00097-1

Yang, C. M. (2001). Sediment distribution in the northern Huatung Basin (Master Thesis). Retrieved from https://hdl.handle.net/11296/bfh9wg. Taiwan: National Taiwan University.

Yeh, K. Y., & Cheng, Y. N. (2001). The first finding of Early Cretaceous radiolarians from Lanyu, the Philippine Sea plate. *Bulletin-National Museum of Natural Science*, *13*, 111–146.

Yu, S. B., Chen, H. Y., & Kuo, L. C. (1997). Velocity field of GPS stations in the Taiwan area. *Tectonophysics*, *274*(1–3), 41–59. https://doi.org/10.1016/s0040-1951(96)00297-1

Yue, L. F., Suppe, J., & Hung, J. H. (2005). Structural geology of a classic thrust belt earthquake: The 1999 Chi-Chi earthquake Taiwan (Mw = 7.6). *Journal of Structural Geology*, *27*(11), 2058–2083. https://doi.org/10.1016/j.jsg.2005.05.020

Yue, L. F., Suppe, J., & Hung, J. H. (2011). Two contrasting kinematic styles of active folding above thrust ramps, western Taiwan. In K. McClay, J. Shaw, J. Suppe (Eds.), *Thrust fault-related folding AAPG Memoir* (Vol. 94, pp. 153–186). London: Association of Petroleum Geologists.